Institute of Space and Aeronautical Science, University of Tokyo
Report No. 549, September 1977

The Analysis of Helicopter Roter Noise

By

Yoshiya NAKAMURA

Summary: Rotational noise which is predominant in helicopter noise is decomposed into thickness noise and loading noise by its cause of generation. It is also divided into near field noise and far field noise by its classification of radiating region. Such decomposition of noise sources and separation of an integral solution of wave equation into integrand and integrating region made it possible to predict noise characteristics analytically.

The integrating region named "influential surface" can be determined once observer position and time are specified. All noise sources which will bring the pressure change at the observer simultaneously are distributed in this region.

The influential surface changes its shape dynamically, because the relative velocity of the blade element to the observer varies over the rotor disk. The magnitude of near field noise is propotional to the area of the influential surface and that of far field noise is propotional to its time derivative.

By these decompositions of the integral expression of pressure change it has become possible to predict analytically many noise characteristics such as wave form, noise level, spectrum, and so on, as the function of rotor parameters. Some methods of noise reduction have been proposed based on a parametric study.

The thickness noise is considered to have fairly high noise level and to be one of potential cause of blade slap. The analytical study of the effect of blade-vortex interaction on the slap has been left for future investigation.

NOMENCLATURE

$A(\boldsymbol{y}, \tau)$	source distribution function
B	number of blades
C	chord length
D	drag, kg
ΔD	drag per unit area of blade, kg/m^2
d_i	acoustic dipole, kg/m^3
$F(\boldsymbol{y}, \boldsymbol{x}, t)=0$	$(=f(\boldsymbol{y}, \tau)=f(y, t-[r]_{\mathrm{ret}}/c))$ equation of influential surface
$f(\boldsymbol{y}, t)=0$	equation of body surface
f_η	f in the η-frame
$G(r, t)$	Green's function
$g=0$	$(=\tau-t+[r]_{\mathrm{ret}}/c)$, equation of acoustic sphere
$h(\eta_1)$	blade height from chord line
L	lift, kg
ΔL	lift per unit area of blade, kg/m^2

M	$(=\boldsymbol{y}/c)$, Mach number of source motion
M_r	$(=\boldsymbol{v}\cdot\boldsymbol{n}/c=v_r/c)$, relative Mach number of source motion to observer
M_t	$(=R\Omega/c=V_t/c)$, rotor tip Mach number
m	acoustic monopole, kg/m^4
N	time order
$\boldsymbol{N}=(N_1,N_2,N_3)^T$	unit vector outward normal to influential surface
$\boldsymbol{n}=(n_1,n_2,n_3)^T$	unit vector outward normal to body surface
P_{ij}	stress tensor, kg/m^2
p	pressure, kg/m^2
p_b	pressure on blade surface, kg/m^2
p_1	thickness noise (monopole noise), kg/m^2
p_2	loading noise (dipole noise), kg/m^2
p_{2T}	thrust noise (dipole noise), kg/m^2
p_{2D}	drag noise (dipole noise), kg/m^2
p_{2F}	far field noise (dipole noise), kg/m^2
p_{2N}	near field noise (dipole noise), kg/m^2
p_{1in}	integrated value of thickness noise source on influential surface
$p_{2TF_{in}}$	integrated value of far field thrust noise source on influential surface
$p_{2DF_{in}}$	integrated value of far field drag noise source on influential surface
$p_{2F_{in}}$	$=p_{2TF_{in}}+p_{2DF_{in}}$
q_{ij}	acoustic quadrupole, kg/m^2
R	rotor radius, m
R_0	blade cut off radius, m
r	$(=\|x-y\|)$, distance between source point and observer, m
$[r]_{ret}$	retarded distance between source point and observer, m
$\hat{\boldsymbol{r}}=(\hat{r}_1,\hat{r}_2,\hat{r}_3)^T$	unit vector in radiation direction (fluid fixed coordinate)
$\hat{\boldsymbol{r}}=(\hat{r}_{\eta_1},\hat{r}_{\eta_2},\hat{r}_{\eta_3})^T$	unit vector in radiation direction (blade fixed coordinate)
S	body surface
dS	element of body surface
T_{ij}	Lighthill's stress tensor
T	thrust, kg
t	observer time, sec
$\boldsymbol{V}=(V_1,V_2,V_3)^T$	rotor hub velocity (fluid fixed coordinate), m/sec
$\boldsymbol{V}_\eta=(V_{\eta_1},V_{\eta_2},V_{\eta_3})^T$	roter hub velocity (blade fixed coordinate), m/sec
V_t	$(=R\Omega)$ rotor tip speed
$\boldsymbol{v}=(v_1, v_2, v_3)^T$	velocity of body
v_n	$(=\boldsymbol{v}\cdot\boldsymbol{n})$ component of velocity outward normal to body surface, m/sec
v_r	$(=\boldsymbol{v}\cdot\hat{\boldsymbol{r}})$ component of velocity of body surface in radiation direction, m/sec
$\boldsymbol{x}=(x_1,x_2,x_3)^T$	observer position vector
$\boldsymbol{y}=(y_1,y_2,y_3)^T$	source position vector
$\boldsymbol{y}_H=(y_{H1},y_{H2},y_{H3})$	position vector of the origin of the η-frame
β	observer azimuthal angle
Γ	curve of intersection of body with acoustic sphere, $g=0$

δ	observer elevation angle
$\delta(\ )$	Dirac's delta function
η_i	blade fixed Cartesian coordinates (Fig. 2–1)
$\Delta\eta$	parameter denoting the mesh size of numerical integration in space
θ	angle between $\boldsymbol{n}$ and $\hat{\boldsymbol{r}}$
θ_0	collective pitch angle
ρ_0	density of undisturbed fluid, kg·sec/m^4
Σ	influential surface
τ	source time, sec
$\tau_2-\tau_1$	time spent for acoustic sphere, $g=0$, to cross body at fixed observer position, $\boldsymbol{x}$ and observer time, t
ϕ	angle between η_1- and y_1-axis
ψ	blade azimuthal angle
Ω	rotor rotational speed, rad/sed
μ	$(=V/R\Omega)$, advance ratio
λ	see equation (2–7)

superscrit

$(\ )^T$	Transposed form of $(\ )$

subscripts

$[\ ]_{ret}$	value at retarded time
$(\ )_{in}$	integrated value on influential surface
$(\hat{\ })_m$	m th order component of Fourier series
$(\ )$	fluid fixed coordinate
$(\ )'$	Lolentz transformed coordinate
$(\ )''$	$(=(\ )'/\sqrt{1-M^2})$

operator

∇	$(=\partial/\partial x_i)$, nubra operator
∇^2	$(=\partial^2/\partial y_1^2+\partial^2/\partial y_2^2+\partial^2/\partial y_3^2)$, Laplacian operator
$\Box$	$(=1/c^2(\partial^2/\partial t^2)-\nabla^2)$, wave operator

1. Introduction

Recently, the aircraft noise has become a serious social problem [*1*, *2*], and the effort to alleviate this public nuisance has been made in both engineering and political fields. The research work to reduce jet-engine noise has been achieved to some degree by many investigators [*3–10*]. The night operation of the aircraft is limited in almost all major airports and newly planned airports are requiered to locate far from the city center. Thus, there is a growth of needs for quiet transportation systems connecting among the city centers and the city center to the airport.

In this regard, the helicopter is a more ideal candidate than other V/STOL systems because of an inherent characteristics of the lowest disk loading in the aircraft. The noise level of helicopter is very much small comparing with the jet planes, but its influence to our community is not so small because the helicopters fly over frequently near the city center or our residence region at lower altitude than others. Recently,

a movement for the establishment of helicopter noise certification has become active [*11–14*], and then it is expected to study about the helicopter noise characteristics such as its cause, character of tone, influence to our life, and the way of reduction.

The rotor rotational noise is the most predominant one in the helicopter noise. By spectrum analysis, the rotor noise can be decomposed into a rotational noise which has a line spectrum based on the harmonics of blade passing frequency and a broad hand noise generated in the boundary layer of airfoil or in its wake. The former is dominant in low frequency range and the latter is so in high frequency range. However, once a violent noise called "blade slap" which is a strong pulsating noise peculiar to helicopter occurs, it overcomes other noise. Although the cause of slap has been thought to be a blade-vortex interaction [*15–19*], the blade thickness effect is also a probable source [*20–24*].

Since the study of rotor noise was initiated by Gutin for propellar [*26*], his "harmonic method" has been extended to noise analysis related to the rotational blade such as helicopter rotor by many investigators [*27–49*]. This method has, however, a disadvantage essentially in calculating the helicopter rotor noise in forward flight, because it needs a condition of the relative stationarity of the rotor position with respect to an observer to expand the rotating noise source in Fourier series.

In this report, a method of direct integration of distributed sources on an "influential surface or surfaces" will be introduced. This method is an extension of the Farassat's result to calculate the blade rotational noise of helicopter rotor and is convenient to predict many noise characteristics analytically.

2. Formulation

2-1 Wave Equation and Its Solution

The sound pressure generated by a moving source is, from Ffowcs Williams & Hawkings [*50–53*], given by the following linear wave equation:

$$\Box p \equiv \frac{1}{c^2}\frac{\partial^2 p}{\partial t^2} - \nabla^2 p = \frac{\partial}{\partial t}[\rho_0 v_n |\nabla f| \delta(f)] - \frac{\partial}{\partial y_i}\left[P_{ij} \cdot \frac{\partial f}{\partial y_j} \cdot \delta(f)\right] + \frac{\partial^2}{\partial y_i \partial y_j} T_{ij}, \quad (2\text{-}1)$$

where the left hand side of the above equation denotes the wave propagation and the right hand side shows source terms, in which the first and second terms are respectively based on blade thickness and pressure distributions and the third term is based on Lighthill's stress distributions in the boundary layer around the blade surface or in the wake. They are corresponding to acoustic monopole, dipole, and quadrupole respectively.

Here, we want to neglect the effects of fluid viscousity and Raynolds' stress in source terms by considering their unimpotance in the rotor noise, and effects of sound reflection, deflection, and diffraction in the radiation field for simplicity of the calculation.

Then equation (2-1) becomes

$$\Box p = \frac{\partial}{\partial t}[\rho_0 v_n |\nabla f| \delta(f)] - \frac{\partial}{\partial y_i}\left[p_b \frac{\partial f}{\partial y_i} \delta(f)\right]. \quad (2\text{-}2)$$

A solution of equation (2-2) may be decomposed into two parts, thickness noise and

loading noise, each of which satisfies respectively the following equations:

$$\Box p_1 = \frac{\partial}{\partial t}[\rho_0 v_n |\Gamma f| \delta(f)], \tag{2-3}$$

$$\Box p_2 = -\frac{\partial}{\partial y_1}\left[p_b \frac{\partial f}{\partial y_i}\delta(f)\right]. \tag{2-4}$$

Having applied to the pressure field generated by a helicopter rotor, these equations can be solved as follows [*21–23*]:

$$p_1(\boldsymbol{x}, t) = \frac{\partial}{\partial t}\rho_0 c \int_{\tau_2}^{\tau_1}\int_{\Gamma} \frac{(V_1 \sin\psi - V_2 \cos\psi + r_{\eta 2}\Omega)\cdot \partial h/\partial r_{\eta 1}}{4\pi r \lambda} d\Gamma d\tau, \tag{2-5}*$$

$$p_2(\boldsymbol{x}, t) = \frac{\partial}{\partial t}\int_{\tau_2}^{\tau_1}\int_{\Gamma} \frac{-\hat{r}_{\eta 3}\cdot \Delta L + \hat{r}_{\eta 1}\cdot \Delta D}{4\pi r \lambda} d\Gamma d\tau + c\int_{\tau_2}^{\tau_1}\int_{\Gamma} \frac{-\hat{r}_{\eta 3}\cdot \Delta L + \hat{r}_{\eta 1}\cdot \Delta D}{4\pi r^2 \lambda} d\Gamma d\tau, \tag{2-6}*$$

where

$$\lambda^2 = 1 - \hat{r}_{\eta 3}^2 + (\partial h/\partial r_{\eta 1})^2 (1 - \hat{r}_{\eta 1})^2 \tag{2-7}$$

$$\hat{r}_{\eta 1} = (r_1/r)\sin\psi - (r_2/r)\cos\psi \tag{2-8}$$

$$\hat{r}_{\eta 3} = (r_3/r), \tag{2-9}$$

and where

τ_1; source time at which the acoustic sphere enters the body of noise sources,
τ_2; source time at which the acoustic sphere leaves the body of noise sources.

Fig. 2–1 shows two coordinate systems used in the present calculation, one of which is fluid fixed coordinate system, $\boldsymbol{y}$, and the other is blade fixed coordinate system, $\boldsymbol{\eta}$.

Since the loading noise consists of two parts by the order of r (distance between source and observer) in the denominator of equation (2-6), far field noise and near field noise,

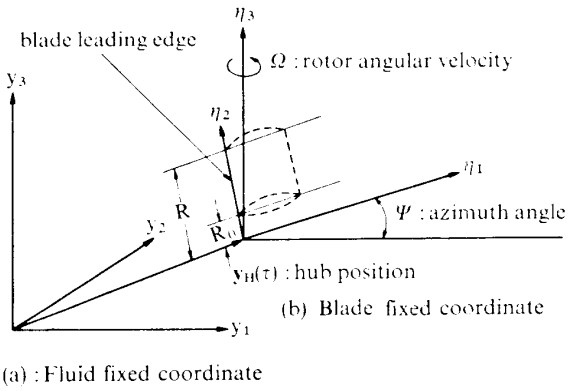

FIG. 2-1. Coordinate Systems used in the Present Analysis

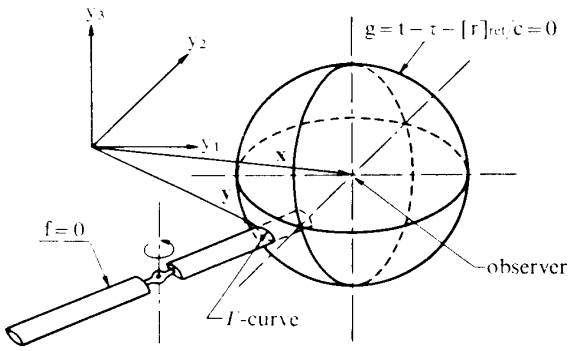

FIG. 2-2. Formation of Γ-Curve by the Intersection of a Collapsing Sphere, $g=0$, and a Body (Blade), $f=0$.

* The integration $\int_{\Gamma} d\Gamma$ should be performed on the rotor disk.

and the integrand of the respective part is also divided into two kinds of noise sources, local lift, ΔL, and local drag, ΔD, it can be said finally that the rotational noise of helicopter rotor is composed of five components of noise sources;thickness noise, p_1, far field thrust noise, p_{2TF}, near field thrust noise, p_{2TN}, far field drag noise, p_{2DF}, and near field drag noise, p_{2DN}.

One of the main purpous of this paper is to investigate the variation of noise level of these five components with various rotor parameters.

It is shown in equations (2-5) and (2-6) that the respective solution contains observer time derivative, $\partial/\partial t$, integration along Γ-curve and integration along source time, τ, where Γ is the intersection line of an acoustic sphere, $g=t-\tau-[r]_{rei}/c=0$, with external surfaces of bodies considered to be noise sources (blade surfaces), $f(y, \tau)=0$. As shown in Fig. 2–2 the acoustic sphere contracts towards an obsever with the speed of sound, c, whereas the blades rotate around the rotor axis as the time is elapsing. Therefore Γ and τ are considered to be functions of the observer time and position.

In order to calculate the noise field of a moving source, the concept of retarded time must be considered, because the pressure change at different points and times can be received by the observer simultaneously.

It is, thus, useful to know all regions of noise sources that have influence on the observer at a given time and position. These regions will be formed by the trajectories of the Γ-curves of the given observer time and position with the change of the source time, $-\infty<\tau\leq t$.

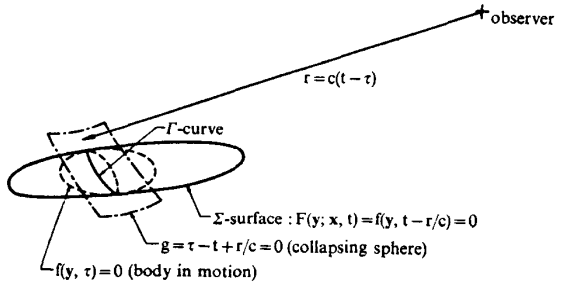

FIG. 2-3. The Collapsing Sphere $g=0$ in the Process of Intersecting the Moving Body $f(y, \tau)=0$ and Forming the Γ-Curve. The Σ-Surface Is the Surface Generated by all Γ-Curves as the Source Time τ Varies from $-\infty$ to t for Fixed Observer Position x and Time t.

An external surface of each of these regions is named "Influential Surface" and is shown in Fig. 2–3 as $F(x, t)=0$. All sources distributed on this surface must be integrated to give the instantaneous pressure of the given observer time and position in equations (2-5) and (2-6). By considering the shape of the influential surface, many characteristic effects of various parameters on each noise component will be predictable analytically as will be explained in 4.

2-2 *Source Time and Observer Time*

Here, let us consider a relation between the source time, τ, and the observer time, t. The source time is a retarded value of the observer time;

$$\tau = [t]_{ret} = t - [r]_{ret}/c \tag{2-10}$$

where $[r]_{ret}$ is the retarded distance between observer and source positions.

By assuming the distance, r, is so large that the acoustic sphere can be considered a plane, the following relation will exsist:

$$r = r_0 + R\cos(\Omega t)$$

Then, it can be resulted the following relations:

$$t = \tau + (R/c)\cos(\Omega t) + (r_0/c) \tag{2-11}$$

$$dt/d\tau = 1 - M_t \sin(\Omega t) \tag{2-12}$$

where c is the sound speed and $M_t(=R\Omega/c)$ is a rotational tip Mach number.

For the rotor, moving with subsonic tip speed, or $M_t<1$, t is a monotone-increasing function of τ, but for the rotor moving with supersonic tip speed, or $M_t>1$, t takes plural values of τ as shown in Fig. 2–4.

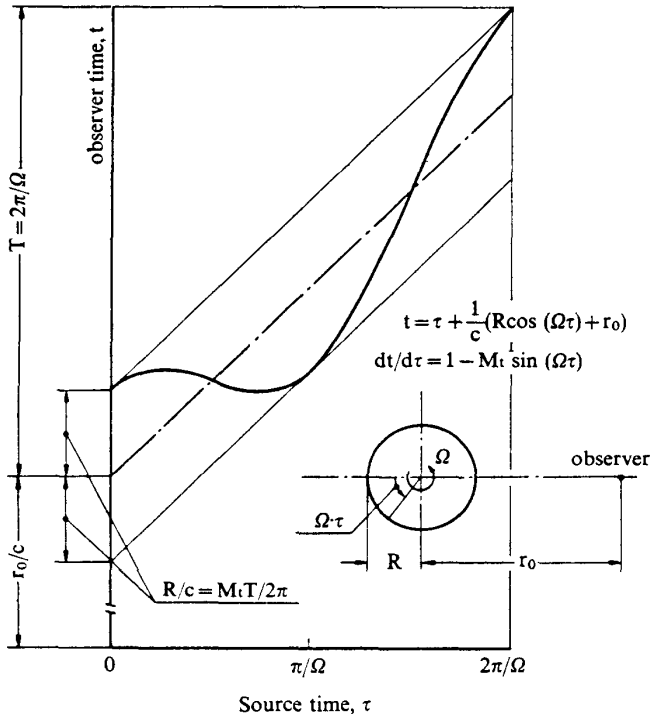

FIG. 2-4. An Example of a Relation Between Source Time and Observer Time

2-3 *Multiplying Factors for a Moving Source*

The solution of wave equation for a moving source can be obtained by multiplying the solution for static source, $q/4\pi r$, with a motion factor which changes its form corresponding to the coordinate systems adopted. It is analogous to the electro-magnetic field produced by a moving electron, the solution of which is known as the Liénard-Wiechart potential [*54*].

Let us consider a point source, $q(t)$, moving with uniform velocity, V, with respect to the surrounding fluid. The source distribution density can thus be expressed as:

$$q(t)\delta(x_1 - Vt)\delta(x_2)\delta(x_3)$$

where $\delta(\ )$ is the Dirac's delta function. Then the wave equation for the sound pressure field produced by the above moving source is of the form,

$$\frac{1}{c^2}\frac{\partial^2 p}{\partial t^2} - \nabla^2 p = q(t)\delta(x_1 - Vt)\delta(x_2)\delta(x_3)\,. \tag{2-13}$$

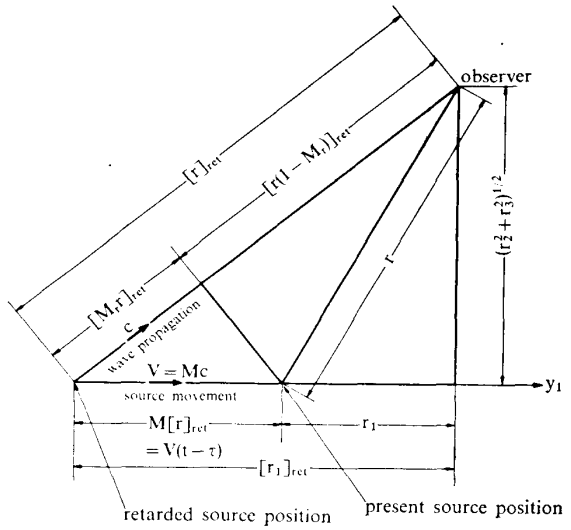

FIG. 2-5. Geometrical Representation of Retarded Values

The solution of this equation is, in the fluid fixed coordinate system, given by

$$p(\boldsymbol{x}, t) = [q(t)/4\pi r(1 - M_r)]_{ret} . \tag{2-14}$$

This solution shows that the stationary solution is strengthen by a factor of $1/(1-M_r)$ because of source motion. The observed noise generated by a moving source is equivalent to the noise by a stationary source locating at an apparent position whose distance is shorten by the factor of $1/(1-M_r)$ (Fig. 2–5).

This may be rewritten in a Lorentz transformed coordinate system (expressed by a single prime) as

$$p(x, t) = \frac{q\{(t' \mp r'/c)/\sqrt{1 - M^2}\}}{4\pi r'(1 - M^2)^{3/2}} \tag{2-15}$$

which can also be rewritten by an elongated transformation such as $(\ )''=(\ )'/\sqrt{1-M^2}$,

$$p(x, t) = \frac{q(t'' \mp r''/c)}{4\pi r''(1 - M^2)} , \tag{2-16}$$

Each solution given by equation (2-14), (2-15) and (2-16) has a corresponding multiplying factor based on the source motion; $[1-M_r]_{ret}^{-1}$, $(1-M^2)^{-3/2}$, $(1-M^2)^{-1}$, respectively. The difference among these factors is caused by the differnce of the coordinate system the solution of which is denoted.

3. Analytical Prediction

3-1 A Method of Prediction

Let us split the solution (2-5) or (2-6) into three items: 1) integrand, 2) integral region, 3) observer time derivative. These will be respectively studied by means of 1) source magnitude 2) integral effect, 3) differential effect, as follows:

1) Source Magnitude

a) Thickness noise—The numerator of the integrand of equation (2-5) is the multiplication of chordwise rate of blade thickness, $dh/d\eta_1$, and the local speed of blade element, $V_1 \sin\psi - V_2 \cos\psi + \eta_2\Omega$. The value of $\partial h/\partial\eta_1$ depends on the shape of airfoil section and the thickness ratio of the blade or wing at the influential surface. For example, the NACA 4-digit airfoil has the value of infinity at the leading edge (Fig. 3–1), whereas the double parabollic airfoil has a linearly decreasing value all over the chord. In general, $\partial h/\partial\eta_1$ is positive in the front part of airfoil, and is negative in the rear part. The local speed of blade element is highest at the blade tip of advancing side, and increases with the rotor rotational speed or rotor advancing speed. Thus,

the blade tip at the highest speed, specifically at the leading edge, has an important role for the generation of the thickness noise.

b) Loading Noise—The numerator of the integrand of equation (2-6) is the multiplication of the directivity parameter, $\hat{r}_{\eta_i}$, and the local blade loadings (local thrust and drag per unit area of the blade), ΔL and ΔD. The aerodynamic loading increases with the square of the rotor rotational speed, and with the increase of collective pitch angle. It is thus understood that the tip region of blade advancing side is again important for the generation of the loading noise. Generally speaking, the more the sources are concentrated, the bigger the noise become, because the change of integrated value on the influential surface increases with source concentration.

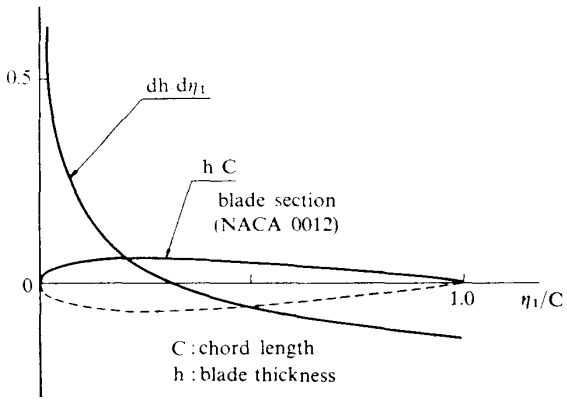

FIG. 3-1. Chordwise Monopole Distribution for NACA 0012 Airfoil

2) Integral Effect

The influential surface is an integral region in the fluid fixed coordinate so that the integral effect depends on the shape and the scale of the influential surface.

Let us consider for simplicity that the sources are distributed on a line named "source line", instead of a rotor blade, rotating around its one end and that the observer locates at the infinite distance from the rotor in the rotor plane. Fig 3–2 (a) shows an "influential line" of the rotor having subsonic tip speed. An acoustic sphere sweeps a moving rotor plane towards the observer from infinite distance, and intersects with the rotor plane on a moving line, named "acoustic line", as the time is elapsing. By considering a case that the acoustic sphere hits the blade at just opposite side of the observer in the

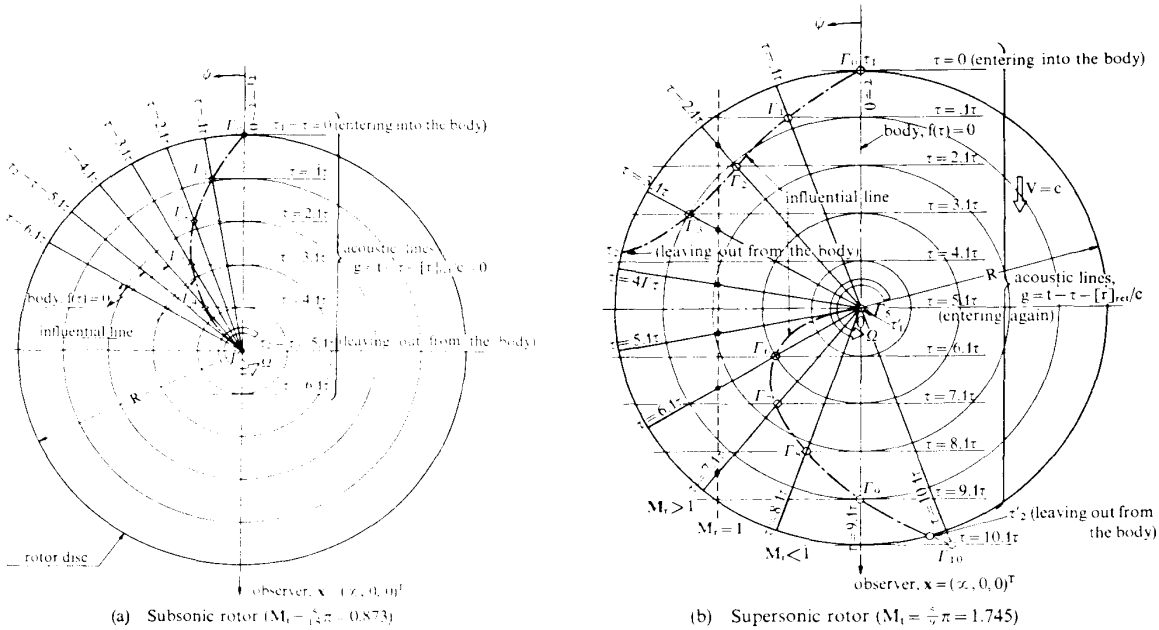

(a) Subsonic rotor ($M_t = \frac{5}{7}\pi = 0.873$) (b) Supersonic rotor ($M_t = \frac{5}{9}\pi = 1.745$)

FIG. 3-2. Formation of Influential Line for a Given Observer Position x and Time t.

rotor disk ($\psi=0°$), an initial starting point of the influential line is apparently specified by Γ_0 as shown in Fig. 3–2 (a) for the subsonic rotor and in Fig. 3–2 (b) for the supersonic rotor. At the subsequent time elapsed by $\Delta\tau$, the acoustic line moves towards the observer by the distance of $\Delta\tau \cdot c$, and the blade or the source line rotates by the angle of $\Delta\tau \cdot \Omega$. Then the point of intersection of both lines will occupy Γ_1 on the influential line. By connecting these points of intersection successively, the influential line will be constructed as a chain line in each of Fig. 3–2 (a) and (b). The sources distributed on this line are considered to be accumulated to produce the pressure observed at a

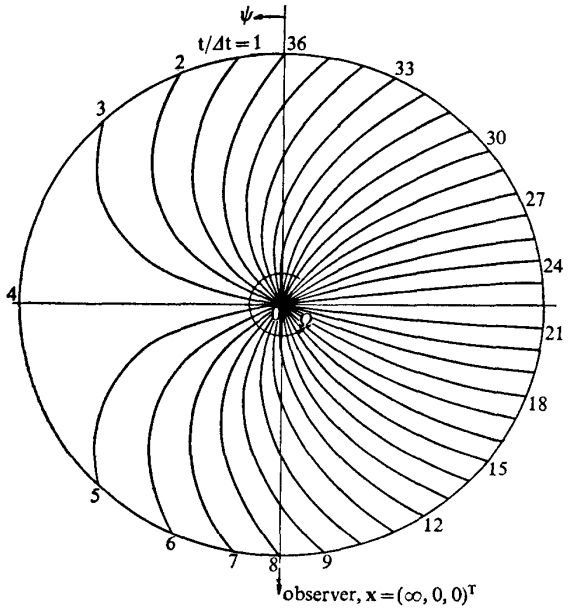

(a) Subsonic rotor, $M_t<1$, and the observer is at infinity. ($M_t=\frac{5}{18}\pi=0.873$ and $\Delta t=R/5c=M_t/5\Omega$)

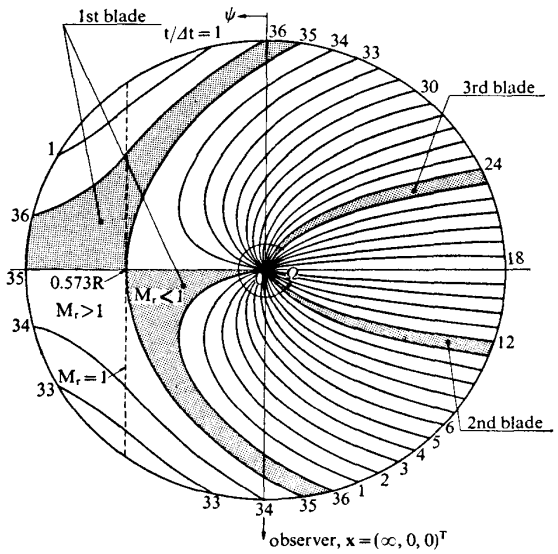

(b) Supersonic rotor, $M_t>1$, and the observer is at infinity. ($M_t=\frac{5}{9}\pi=1.745$, and $\Delta t=R/10c=M_t/10\Omega$)

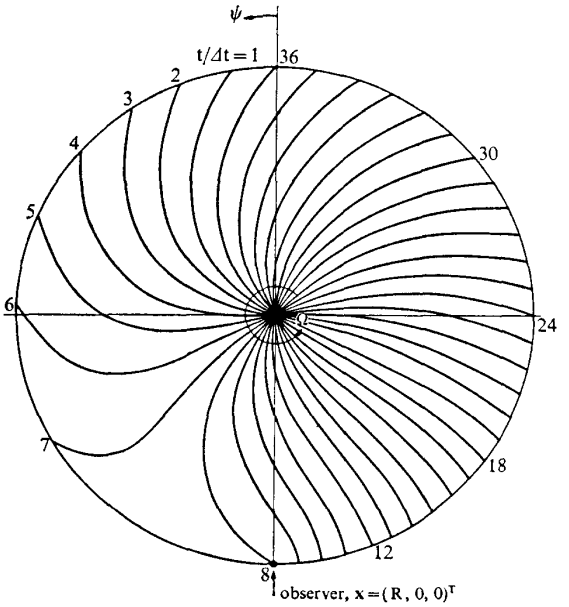

(c) Subsonic rotor, $M_t<1$, and the observer is at rotor edge. ($M_t=\frac{5}{18}\pi=0.873$, and $\Delta t=R/5c=M_t/5\Omega$)

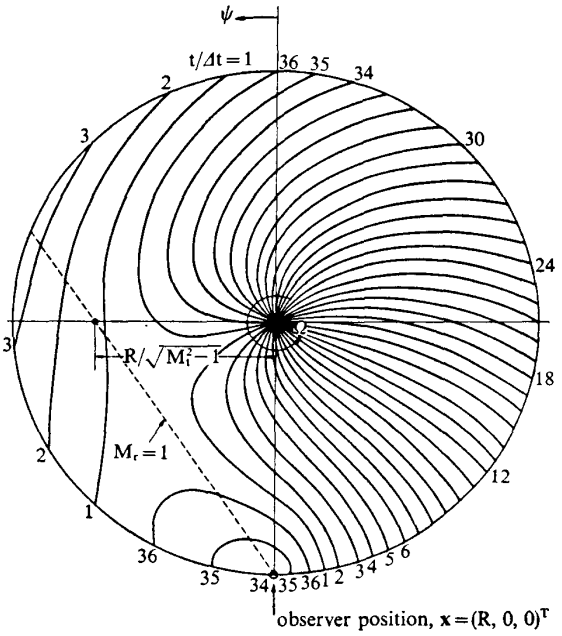

(d) Supersonic rotor, $M_t>1$, and the observer is at rotor edge. ($M_t=\frac{5}{9}\pi=1.745$ and $\Delta t=R/10c=M_t/10\Omega$)

FIG. 3-3. Influential Lines (constant observer time interval)

given time and position.

In Fig. 3–2 (b) a dotted line indicates a boundary outside of which the relative speed of the blade to the observer is supersonic, or $M_r > 1$. The observer is considered to locate at an extended terminal of this rectilinear dotted line. It will be appreciated that the rotation of the rotor blade the influential line approaches to the rotor center in the inside part of this line and leaves to a some point at the rotor edge in the outside part.

A few examples of the influential lines, which are equally spaced by either the observer time or source time, are shown in Fig. 3-3 (a)–(d) as the function of blade tip speed and of the observer position. It can be said that as an area enclosed by two neighbouring influential lines of each figure, in which the influential lines are drawn with equally spaced observer time, becomes larger, the noise energy perceived by the observer is more strongly concentrated. It is, from these figures, shown that the tip region of approaching side of the rotor disk toward the observer ($\psi = 90°$) is the most elongated area, therefore, the most predominant area for the noise generation.

The above area enclosed by two influential lines may be considered as an "influential surface" of the blade by replacing the leading edge and the trailing edge of the blade with the two influential lines, having provided approximately that the planform of the blade is not rectangular but pie shaped. This approximate replacement of the blade planform with the pie shaped area is very much adequate in the noise calculation because the most important region of the noise generation is near the blade tip. An example of the influential surface of a three bladed rotor having supersonic tip speed is shown in Fig. 3-3 (b).

3) Differntial Effect

It has been shown from equations (2-5, 6) that the far field noise can be obtained by integrating the sources on the influential surface and by differentiating the result with respect to the observer time. It is, thus, important for noise generation that not only how large the influential surface is, but also how the influential surface deforms with the observer time. The deformation of the influential surface with time depends on various parameters; rotor radius, blade cut-off, blade planform, blade number, rotor rotational speed, advance ratio, observer position, and so on.

3-2 Prediction of Wave Form

Next example of successful results of analytical prediction by using present consideration by means of the influential surface is a wave form. Since the acoustic pressure of respective noise component can be treated independently each other, an instantaneous pressure is obtainable by summing up or superposing the all noise components.

Here, let us suppose that an observer locates at an infinite distance from the rotor hub (Fig. 3-4).

1) Thickness Noise

A chordwise symmetric airfoil like double parabolic has an antisymmetric source distribution such as positive thickness noise in the front half of the blade and of negative in the rear half. The influential surface of this blade has, as shown in Fig. 3-4 (a), the maximum rate of elongation at $\psi = 90°$, whereas in the before and after region of which the rate of elongation decreases as the blade gets away from $\psi = 90°$.

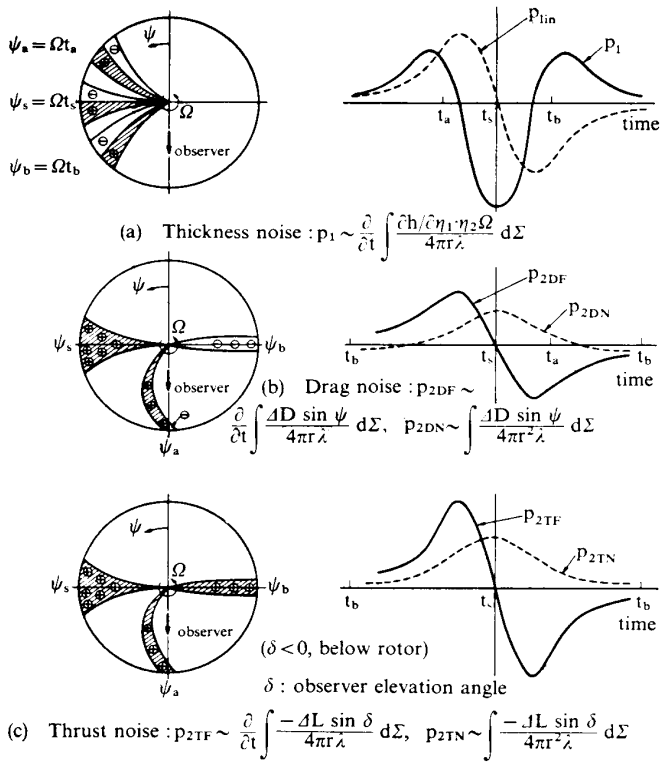

FIG. 3-4. Acoustic Waveform of Each Component for Rotating Single Blade

At $\phi=90°$, the elongation of the influential surface is symmetric so that the positive part of the source distribution is equal to the negative part. At $\phi=\phi_a<90°$, however, the elongation of the influential surface of positive part, $\phi>\phi_a$, is larger than that of negative part, $\phi<\phi_a$; and vice versa at $\phi=\phi_b>90°$. Thus the integration of all sources on the influential surface, $p_{1_{in}}$, gives a positive value at $\phi=\phi_a>90°$, zero at $\phi=90°$, and a negative value at $\phi=\phi_b>90°$, as shown by a dotted line in the right hand side of Fig. 3-4 (a). Then the pressure, which is given as a time derivative of the above integration, has the symmetric change as shown by a solid line in the same figure.

For example, if the observer approaches to the rotor axis, the deformation of the influential surface with time comes to be small. For the observer locating on the axis, the influential surface is not affected by the rotor rotation and hence the far field noise doesn't propagate to the direction normal to the rotor plane.

The observer locating on the rotor plane, on the other hand, maximizes the deformation of the influential surface and thus the far field noise is expected to propagate strongly to the direction of the rotor plane.

In fact these directivities are acertained by the present computation as follows: the thickness noise (monopole; isotropic in all direction) and the far field drag noise (dipole; parallel to the rotor plane) propagate most strongly to the rotor plane, whereas the far field thrust noise (dipole; normal to the rotor plane) has the maximum intensity in a direction between the rotor axis and the rotor plane. The detail results shall be shown in 5.

2) Drag Noise

Under simillar consideration, the wave form of loading noise can be predicted. The drag noise source is positive on the influential surface in the approaching semicircle,

$0°<\psi<180°$, and is negative in the leaving semicircle, $180°<\psi<360°$. Then the integarated value of the sources on the influential surface, $P_{2DF_{in}}$, which is proportional to the wave form of near field drag noise, p_{2DN}, is maximum at $t=t_s$ as shown by a dotted line in the right hand side of Fig. 3-4 (b). The pressure change due to the drag is given by a time derivative of the above dotted line and is shown by a solid line, and thus, the peak values of which are obtained at two phases that the changing rate of elongated influential surface is maximum. This line shows the wave form of far field drag noise, p_{2DF}.

3) Thrust Noise

The sign of integrated value of the thrust noise source depends only on the observer position (observer elevation angle δ). For the observer locating above the rotor disk (the direction of thrust vector; $\delta>0$), the thrust noise source is negative, and for the obsever locating below the rotor disk the situation will be reversed. Thus the integrated value of source, $P_{2TF_{in}}$, depends on the area of influential surface as shown by a dotted line in the right hand side in Fig. 3-4 (c). As in the case of drag noise, this is proportional to the wave form of near field thrust noise, p_{2TN}. The time derivative of this value is the wave form of far field thrust noise, p_{2TF}, shown by a solid line in the same figure.

In actual case, since the observer locates at some finite distance, the changing rate of the influential surface is higher in $\psi>90°$ than in $\psi<90°$. Hence, the wave form observed in the practical field will be unsymmetric as shown in Fig. 3-5.

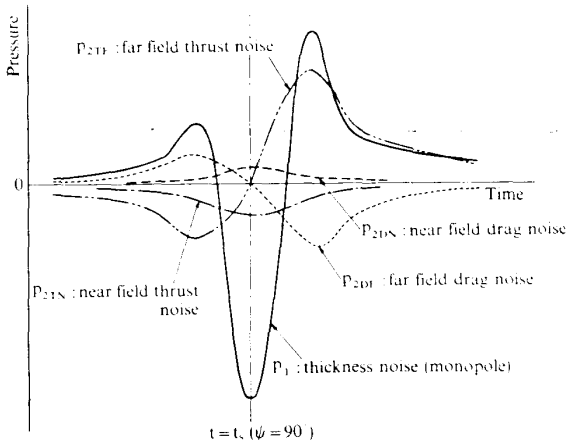

FIG. 3-5. Waveform of Decomposed Rotor Noise (observer locates above the rotor in a finite distance)

3-3 Dimensional Analyses of Sound Level for a Moving Source

Although effects of rotational speed and advance ratio on the sound level will be discussed in 5, it is worthwhile to study the general effects of source speed on the sound level as the preliminary work in this section.

At first let us consider the effect of source speed on the magnitude of noise sources. In the case of helicopter rotor noise, a monopole noise is generated by the rate of volume increment which is propotional to a typical velocity u, whereas a dipole noise is associated with the rate of aerodynamic force which is propotional to u^2. In addition, differentiation with respect to observer time, $\partial/\partial t$, can be put propotional to a rotational speed sensed by the observer, $\Omega/[1-M_r]_{ret}$, or $u/[1-M_r]_{ret}$. Then it is resulted that the source magnitude of a monopole is propotional to u^2, and that of dipole is to u^3. Whereas, by the similar analysis, it can be said that the magnitude of quadrupole is propotional to u^4.

Next, let us extend the present consideration to the moving effect. For the solution of wave equation having a moving source, an amplification factor, $1/[1-M_r]_{ret}$,

should be multiplied to the stationary solution as described before. This is resulted from the elongation of the coordinate system and is represented by the deformation of the influential surface. For the wave equaion of a n th order multipole source, $q_{12}\cdots_n$, the solution is given by;

$$p(x, t)=\frac{1}{4\pi}\int\frac{\partial^n}{\partial x_1\partial x_2\cdots\partial x_n}\left[\frac{q_{12}\cdots_n(t)}{r(1-M)^n}\right]_{ret}dV\,. \tag{3-1}$$

Once the space differentiation (gradient) is operated to the retarded distance, $[r]_{ret}$, an amplification factor $1/[1-M_r]_{ret}$ will be derived as follows;

$$\frac{\partial}{\partial x_i}[r]_{ret}=\left[\frac{r}{r}\cdot\frac{1}{1-M_r}\right]_{ret}. \tag{3-2}$$

By applying n-times space differentiations, the factor $(1/[1-M_r]_{ret})^n$ should be multiplied. From these analyses, the dimensional dependence will be obtained as given by Table 3-1.

TABLE 3-1. Dimensional dependence of acoustic pressure for moving sources

Acoustic source	Acoustic pressure
Monopole	$\left[\frac{u^2}{(1-M_r)^2}\right]_{ret}$
Dipole	$\left[\frac{u^3}{(1-M_r)^2}\right]_{ret}$
Quadrupole	$\left[\frac{u^4}{(1-M_r)^3}\right]_{ret}$

Note: u is a typical velocity of fluid, M_r is a relative Mach number of source to observer.

4. Numerical Calculations and Comparison with the Experimental Results

4-1 Calculation

In making a computer program based on equation (2-5, 6), the following essential assumptions will be introduced:

(i) The sound speed is constant at any point of the fluid so that the sound wave propagates linearly.

(ii) Both the quadrupole source based on Lighthill's stress tensor and viscous effects in the dipole source are neglected.

(iii) The source and the observer are in acoustically free field where reflection or diffraction of the sound wave is out of consideration.

As a rotor model, the following model will be considered for simplicity:

(i) Blade planform is rectanguler.

(ii) Airfoil section is invariant along the span.

(iii) All sources are in the rotor plane.

It has, however, no essential difficulty to remove these limitations in considering other rotor models.

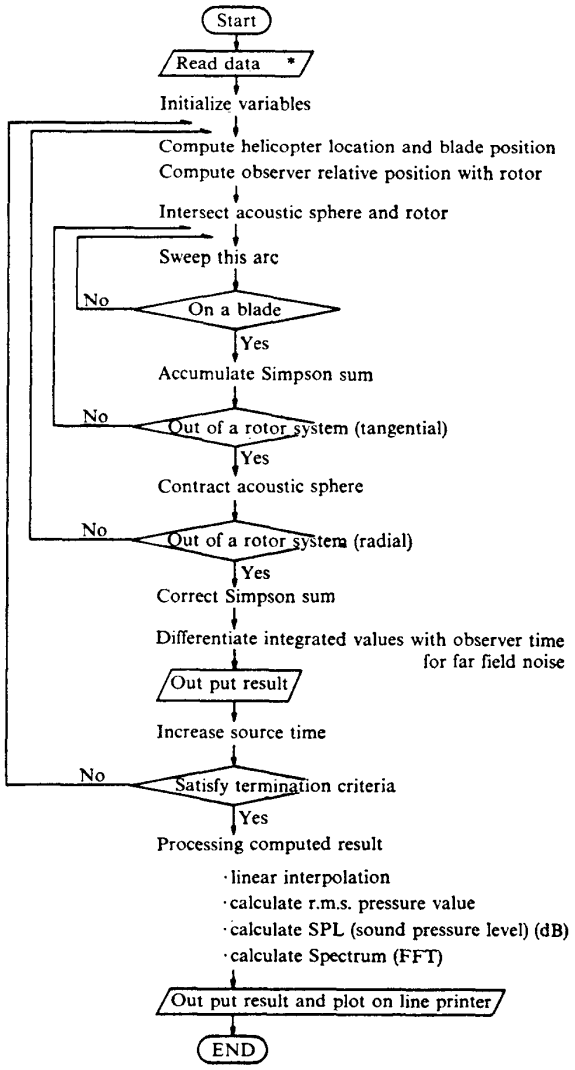

* Data contain rotor geometry, operating conditions, observer position, control parameters, and load distribution computed, for example, by Ref. 45.

FIG. 4-1. Flow Chart of Rotor Noise Program

Fig. 4-1 shows the flow chart of the present program. With sweeping along the arc of polar frame whose origin is an observer point (namely, along the acoustic sphere), the Simpson sum of noise sources is obtained along the arc. As the time elapses this process will be repeated for the new acoustic sphere which has contracted towards the observer. After the acoustic sphere has so fully contracted that it may have left the rotor disk, the radial sum of these Simpson sums gives an integrated value of a given observer time and point such as $p_{1_{in}}$, $p_{2TF_{in}}$, $p_{2DF_{in}}$, p_{2TN}, and p_{2DN}. The far field noise is obtained by taking numerical differentiation of these numerically integrated value, $p_{1_{in}}$, $p_{2TF_{in}}$, and $p_{2DF_{in}}$, with respect to observer time. Then, the accumulation of rounding error is a serious problem as will be discussed next.

The factors which decide the precision level of calculation are:

(i) mesh dimension of the Simpson sum,

(ii) dimension of the observer time increment,

(iii) precision rank adopted in the computation.

1) The Mesh Dimension of Simpson Sum

The double integral of equtions (2-5, 6) is an integration of the influential surface, $d\Gamma d\tau$, where Γ is the intersecting line of the acoustic sphere and the blade surface so that $\int d\Gamma$ is a tangential integration for a fixed source time, τ. As the source time elapses the acoustic sphere contracts and blades rotate. The integration of $\int d\tau$ is considered to be a radial integration. The surface integration may be performed by the Simpson rule, and the dimension of integrating unit is given by a parameter, $\Delta\eta$, which means the value of rotational angle of the rotor blade in the period of the source time increment, $\Delta\tau$. Then the double integration gives a pressure observed at a given time and position.

2) Dimension of Observer Time Increment

By choosing a small increment of the observer time from the initial one, a different influential surface is formed, and a new pressure value can be computed. Continueing this process one after another gives a pressure wave form observed at a given position. A fine increment of the observer time gives a precise wave form, that is to say, this increment scale gives a limitation of the credible order of spectrum in the frequency domain.

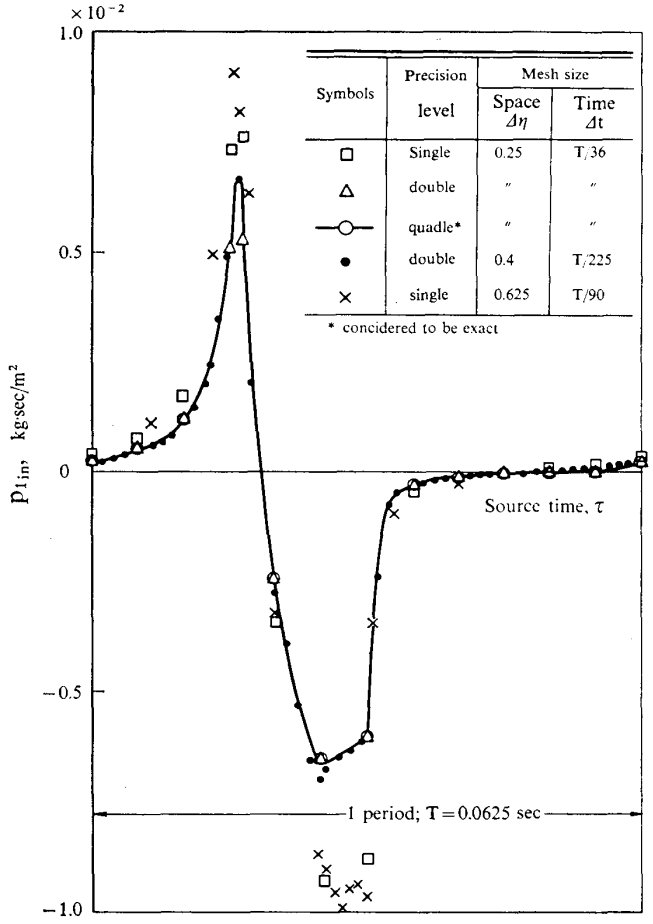

FIG. 4-2. Accuracy of Calculation vs. Data Type or Scale of Summation Interval (p_{1in} vs. source time) for the Rotor (D).

3) Precision Rank Adopted in the Computation

A rounding error will accumulate by the Simpson sum and be enlarged by the differentiation with respect to the observer time. The accumulation of the error increases with the number of summation, though the fine mesh has been considered desirable for the precise computation in the above discussion.

Fig. 4-2 and Fig. 4-3 show a comparison of waveform computed by three kinds of precision level;

(i) single precision (having 8 significant figures),

(ii) double precision (having 19 significant figures),

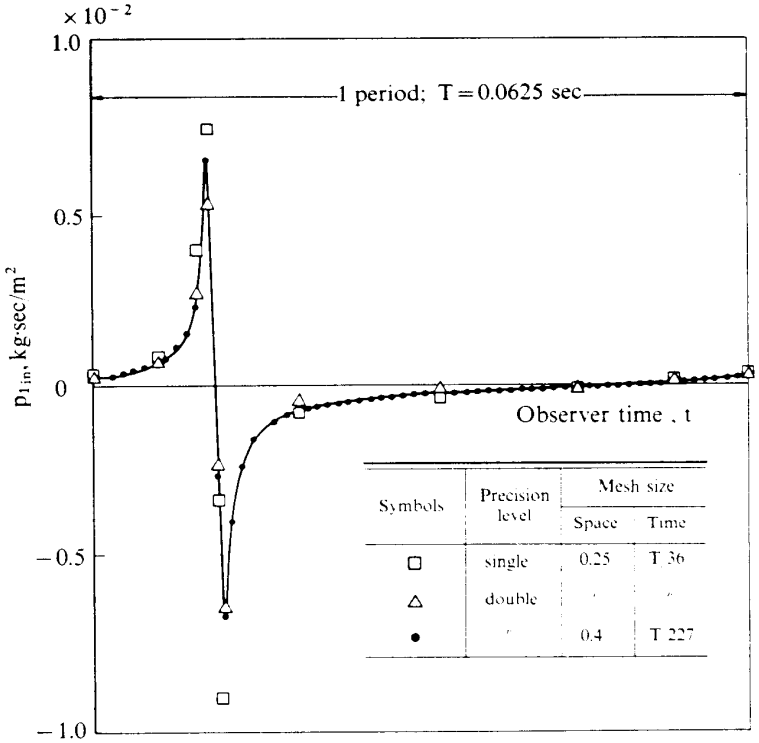

FIG. 4-3. Accuracy of Calculation vs. Data Type or Scale of Summation Interval (p_{1in} vs. observer time) for the Rotor (D)

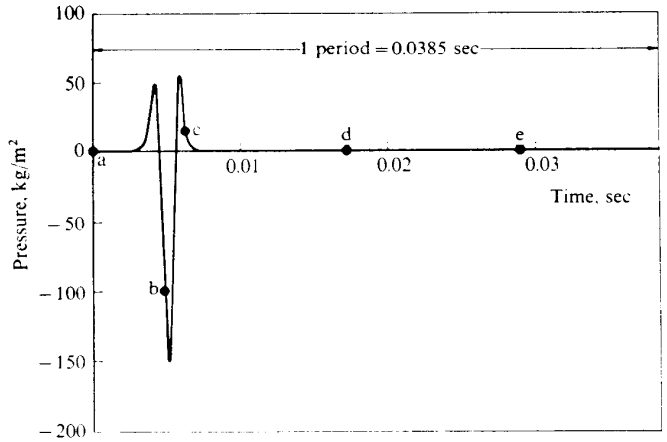

FIG. 4-4. An Example of Acoustic Waveform of Two-Bladed Rotor (A), where Signs a through e Correspond to those in Fig. 4-5

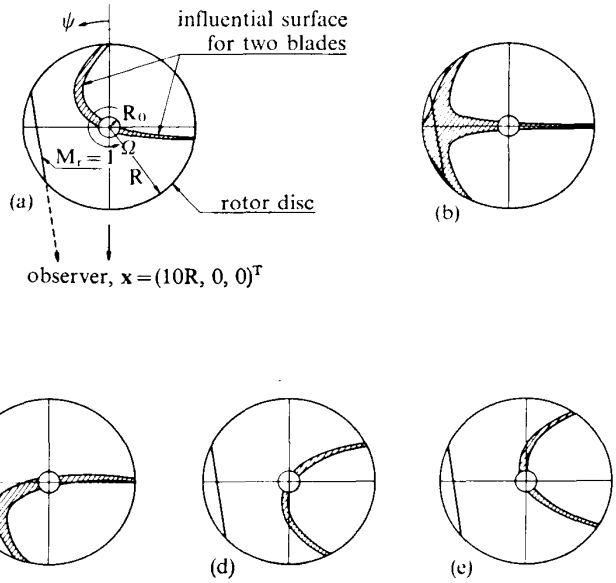

FIG. 4-5. Influential Surface (Tip Mach number; $M_t=1.2$, advance ratio; $\mu=0$, the signs; (a)–(e) correspond to those in Fig. 4-4)

(iii) quadru precision (having 40 significant figures).

The difference between the double precision and the quadru precision is under 0.1%, while the single precision, on the other hand, deviated from the above two values by about 30%. Thus, it is concluded that the double precision is necessary and sufficient for the present calculation.

The necessary value of $\Delta\eta$ for getting reliable integrated results depends on various parameters. Generally speaking, when the area of the influential surface increases namely the relative velocity of source to observer approaches to the sound speed, smaller value of $\Delta\eta$ must be taken to keep the precision level in a good degree.

After some preperatory study to keep sufficient precision level in computation, the number of integrating point was decided. That was about 10^4, which corresponds to the following demension for one element: tangential; chord length/20, radial; rotor radius /300, and $\Delta\eta=0.16$. This mesh dimension requires about twenty seconds to compute the total pressure value of a given observer time and position (the computer used in this calculation was FACOM 230/75). Then it was decided that the number of discrete observer time in the one blade passing period was thirty eight in order to give a total computational time within twenty minutes.

An example of computed wave form is shown by Fig. 4-4. The influential surfaces corresponding to the observer time signed a–e in this figure are shown in Fig. 4–5, in which the point where the pressure changes impulsively corresponds to an azimuthal position where a rapid and great deformation of the influential surface occurs.

Here, it is noted that the dimensions of rotors exemplified in this report are specified in Table 4-1.

4-2 Comparison with Experimental Results

1) Helicopter Rotor Model

The noise of a hovering rotor, whose diamter and number of blades were 2.21 m and

TABLE 4-1. Dimension of exemplified rotors

Item	Dimensions			
	Rotor (A)	Rotor (B)	Propeller (C)	Rotor (D)
Rotor radius, R	5.0 m	1.105 m	0.597 m	6.71 m
Blade cut off, R_0	0.7 m	0.086 m	0.209 m	0.61 m
No. of blades, B	2	4	2	2
Blade chord, C	0.4 m	0.085 m	0.060 m	0.7 m
Tip Mach number, M_t	0.9 or 1.2 (only in specified case)	0.102	1.0 or 1.2	0.992
Advance ratio, μ	0 (hovering)	0	0	0
Observer position, $\|x\|$	50 m ($=10R$)	1.105 m ($=R$)	9.144m ($=15.3R$)	250 m ($=37.3R$)
Elevation angle, δ	0° (in rotor plane)	0°	0° and ±30°	0°
Thickness ratio, h_{max}/C	0.10	0.12	0.06	0.08
Airfoil section	double parabolic	NACA 0012	double parabolic	double parabolic
Thrust, T	1 500 kg	0.8 kg	174 kg	
Torque, Q	1 000 kgm	0.18 kgm	24.7 kgm	
Load distribution used in computation				
chordwise	rectangular	rectangular	rectangular	
spanwise	quadratic	quadratic	quadratic	
azimuthwise	uniform	uniform	uniform	

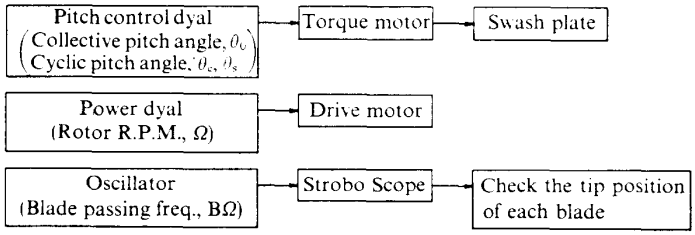

FIG. 4-6 (b). Block Dyagram of Measuring System

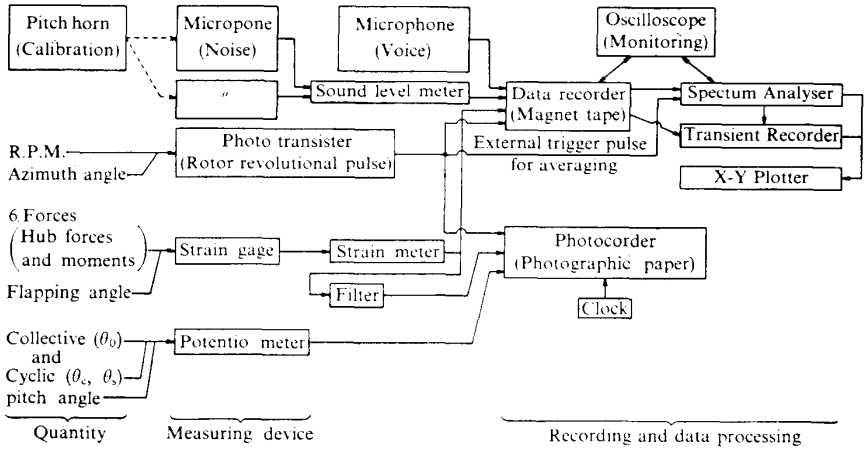

FIG. 4-6 (a). Block Dyagram of Rotor Operating System

two or four respectively, was measured with various rotational speed and thrust. A condensor microphone was located sufficiently near to the rotor to avoid sound reflection or diffraction. Block dyagrams and photographes of rotor system or measurment system are shown in Fig. 4-6–9. The following quantities such as instantaneous pressure change sensed by the condenser microphone, six components of hub forces and moments (thrust, torque, two side forces, pitching and rolling moments), flapping angle sensed by strain gages, and blade azimuthal angle were simultaneously recorded by a magnetic tape.

Based on these input data, the acoustic field was calculated by the present theory and was compared with measured results. Fig. 4–10 shows an example of comparison of computed wave form with measured wave form, and Fig. 4-11 shows a comparison of computed peak-to-peak value of the acoustic pressure amplitude with the experimental result. Through these figures, the coincidence is favorable.

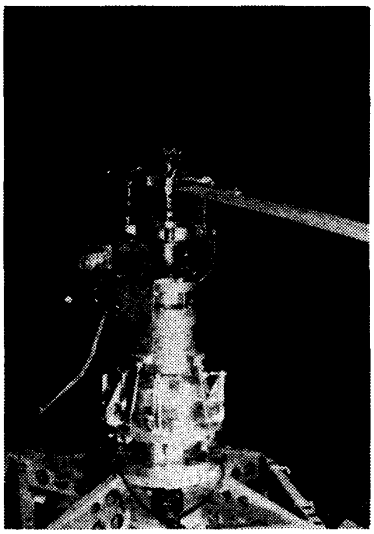

FIG. 4-7. Rotor Model

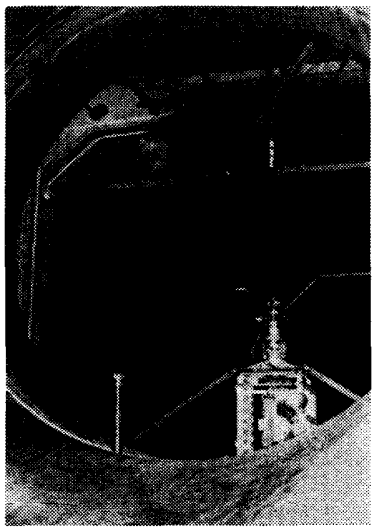

FIG. 4-8. Rotor Model and Microphone

FIG. 4-9. Measuring Instruments

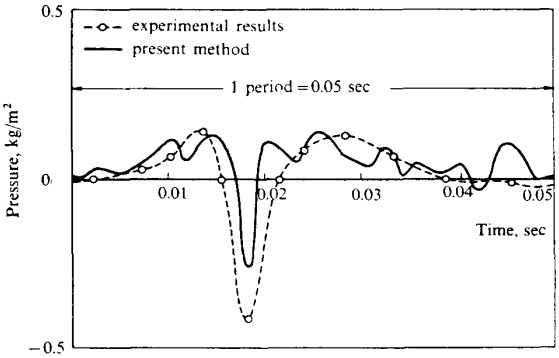

FIG. 4-10. Comparison of Present Theory with Experiment (wave form) for the rotor (B) ($\theta_0 = 4°$)

2) Propeller Model

The present theory was also compared with the experimental results of a static propeller in high tip speed [*58*]. Fig. 4-12 (a)–(d) are comparisons of wave form in the

change of tip Mach number, M_t, and observer elevation angle, δ. The agreement between the measured wave form and the present theory is good.

An effect of tip Mach number at constant power on the over all sound pressure level is shown in Fig. 4-13, where the present theory is compared with not only experimental results but also a harmonic analysis which has been a stereotyped method for the calculation of the rotational noise as described in the subsequent section. The harmonic theory for a rotating-point-force model is shown by black triangles which do not coincide well with the present theory. The harmonic theory for a distributed source model containing thickness effect, which is the same model as that of present theory, is shown by a broaken line which coincides well with the present theory in a very good degree. These results certify the reliability of the present method.

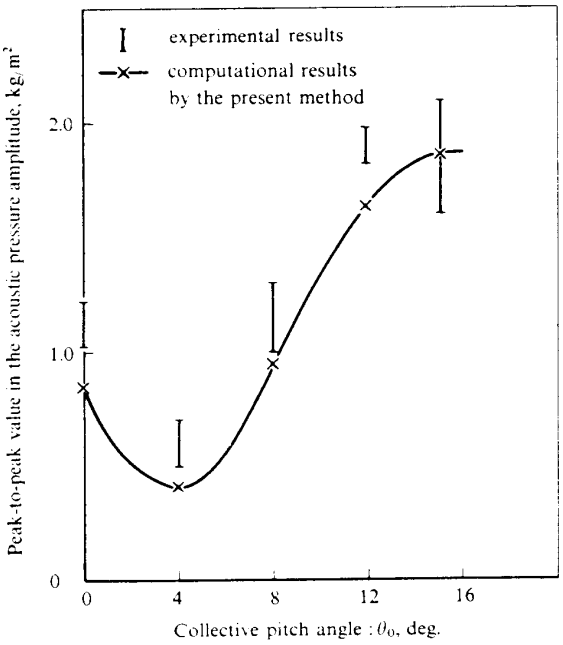

FIG. 4-11. Compariton of Present Theory with Experiment for the Rotor (B)

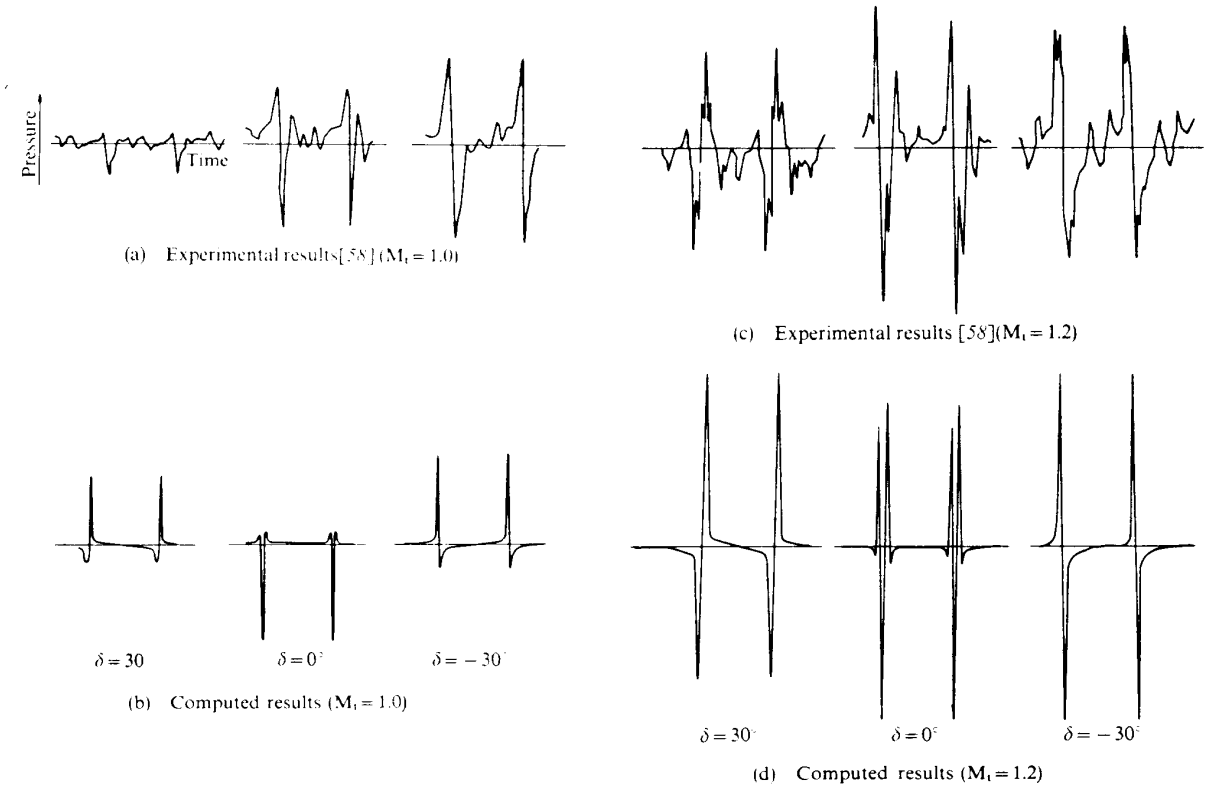

FIG. 4-12. Comparison of Present Theory with Experiment (wave form) for the rotor (C) (M_t=1.0)

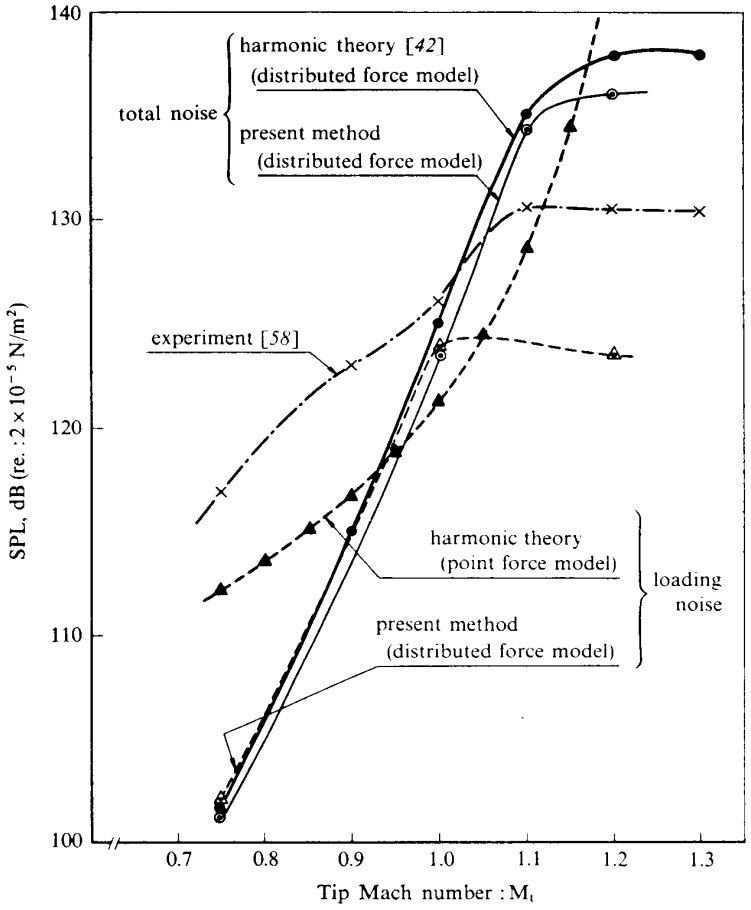

FIG. 4-13. Effect of Tip Mach Number at Constant Power on the Over-all Sound Pressure in Decibels for the Rotor (C) (power loading is equal to 323 HP/m^2)

4-3 Comparison with Previous Theory

Main interest in previous investigators for the rotor noise has been the rotational noise. Gutin [*26*] was the first one opened a way of calculating method for the stationary propeller. Instead of calculating the distributed pressure on a propeller blade, he treated a rotating point force (lift and drag) which could be decomposed into Fourier series.

Under the assumption that a stationary observer locates far from the noise source, which is called "far field approximation", the spectrum of the sound pressure heard by the observer was expressed by a series of Bessel functions. This method shall be called "harmonic theory".

Although Garrick and Watkins [*27*] removed Gutin's restriction of the static propellers by studying the acoustic field of a concentrated force in uniform rectilinear motion, the observer is still in the frame fixed to the rotor. In the nonrotating frame moving with the propeller, only the spectrum of acoustic pressure was obtained by tracing the Gutin's analysis.

Deming [28] studied the effect of the source term involving the normal velocity distribution of the body surface for the static propellers. He utilized Rayleigh's relation for the piston radiation into a semi-infinite space and obtained the acoustic pressure

spectrum. This noise is referred to as the thickness noise. Lyon [*20*] has studied the thickness noise of helicopter rotors in forward flight.

However, it has been true until a recent date that the following restrictions have not been removed: (i) the source is compact, (ii) the relative position of the rotor to the observer is stationary, and (iii) the observer locates in the far field from the noise source.

The assumption of compactness of the source makes a big error when the relative Mach number of the source to the observer approaches to unity. Lowson [*29–34*], Wright [*35–38*], and others [*39–41*] improved the harmonic theory by replacing the model of source from point force to distributed force, from loading noise to both loading noise and thickness noise, but still the assumptions related to the position of source or observer were left.

Based on the wave equation derived by Ffowcs Williams and Hawkings [*50, 51*], Farassat developped a theory for the calculation of the acoustic pressure for bodies in arbitrary motion in the fluid fixed coordinate system, in which the observer is not limited to the far field and no compactness assumption is made [*21, 22*].

In the present paper, by following Farassat's method the acoustic field composed of five kinds of noise sources which were explained in 3 was studied with the special interest of physical point of view.

TABLE 4-2. Comparison of the present theory with the harmonic theory

Items	Present Theory	Harmonic Theory
Noise source	thickness noise and loading noise	mainly loading noise
Source distribution	distributed chordwise spanwise azimuthwise	concentrated
Relative rotor motion to observer	arbitrary	static
Radiating field	arbitrary	farfield
Computation of;		
wave form	suitable	not suitable
peak value	suitable	not suitable
spectrum	not suitable	suitable
Analytical discussion	easy	difficult
Computing time	long	short

Table 4-2 shows the comparison of the characteristics of the present theory with the "harmonic theory". In short, the hormonic theory is a simplified method but has some restrictions, specifically about the rotor motion. The present theory is, on the other hand, one of precise methods with few restrictions, but it takes much computing time. The calculation of fly over noise may be a good example of the application of the present method.

5. Noise Level vs. Various Parameters

In this section, the noise level, or the peak-to-peak amplitude of acoustic pressure is studied for various rotor geometrical parameters such as rotor diameter, blade cut off, number of blades, chord length, shape of airfoil section, and for several operating conditions such as rotor rotational speed, advance ratio, load distribution, and observer position.

Through these calculations, the value of total thrust and torque were kept constant. A standard dimension of computed models is shown in Table 4-1 as rotor (A).

5-1 Rotor Rotational Speed

The dimensional dependence of noise level of the rotating noise source on the source speed is not so easy to know as that of the source in uniform rectilinear motion.

Though relations among the acoustic power of rotor noise, tip speed, and thrust have been proposed by many investigators as shown in Table 5-1 or Fig. 5-1, it has not yet been clearly analyzed.

Table 5-1. Dimensional dependence of acoustic intensity of rotor on tip speed V_t and thrust T [42–49]

Proposer	Acoustic power	Noise considered
Schlegel & Davidson [48]	V_t^2	
Hubbard & Maglieri [48]	$V_t^6 T^2$	low frequency
	$V_t^2 T^2$	high frequency
Goddard & Stuckey [48]	$V_t^8 T^2$	low frequency
	$V_t^2 T^2$	high frequency
Leverton [48]	V_t^6	high thrust near rotor plane
	V_t^8	hight thrust near shaft axis
Wright [38]	V_t^3 (slow)	tip speed, $R_e > 10^6$ (broad band noise generated in turbulent boundary layer)
	V_t^5 (medium)	
	V_t^8 (high)	
The author	$M_t^4/(1-M_t)^4$	thickness noise, p_1
	$M_t^2/(1-M_t)^4$	farfield loading noise, p_{2F} (load const.)
	$M_t^6/(1-M_t)^4$	farfield loading noise, p_{2F} (collective pitch const.)
	$1/(1-M_t)^2$	near field loading noise, p_{2N} (load const.)
	$M_t^4/(1-M_t)^2$	near field loading noise, p_{2N} (collective pitch const).

Note: $M_t = V_t/C$

Here, new dimensional laws have been proposed based on the following considerations: (i) The moving effect of noise source shall be approximated by the elongation of influential surface, $1/(1-M_t)$, where M_t is the tip Mach number. (ii) The differentiation with respect to time in far field noise has a proportional effect to $M_t/(1-M_t)$. (iii) The magnitude of thickness source is proportional to M_t, whereas that of loading

source is proportional to M_t^2 when the collective pitch angle is fixed. When the total loading value is fixed, however, the magnitude of loading source has no dimensional dependence on M_t.

By considering these proportional effects, the following laws will be obtained for the acoustic pressure amplitude of all noise components. (i) The thickness noise is in

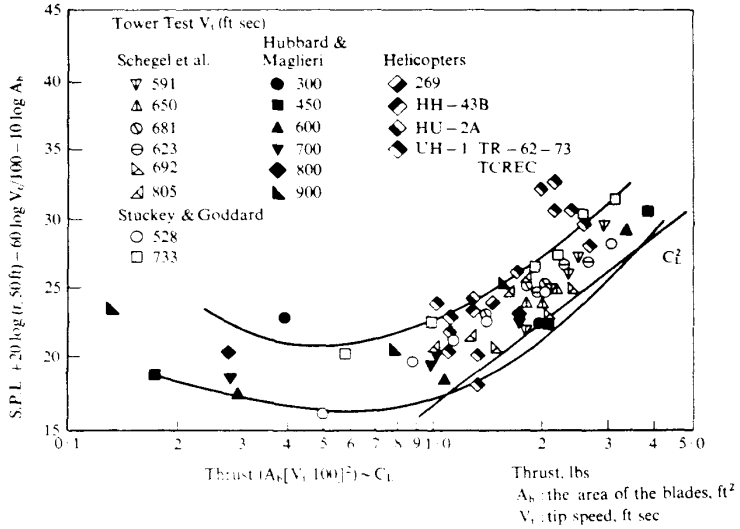

FIG. 5-1. Whirl Tower and Helicopter Vortex Noise. Data from Widnall [*44*]

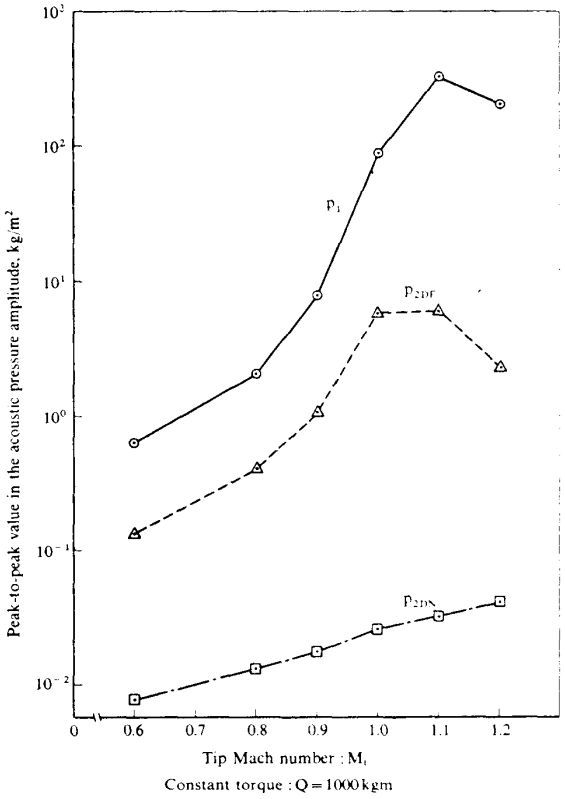

FIG. 5-2. Variation of the Peak-to-Peak Value in the Acoustic Pressure Amplitude vs. Tip Mach Number for the Rotor (A)

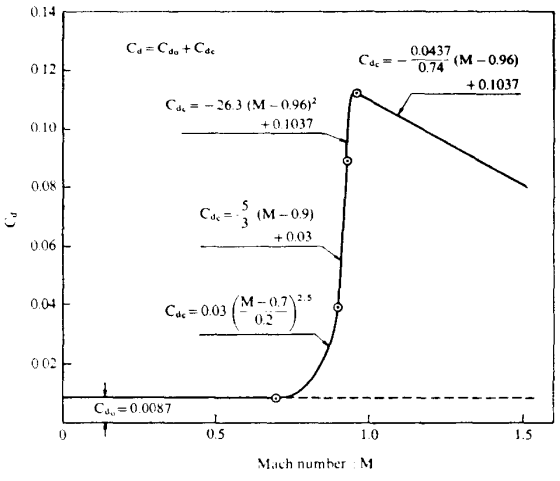

FIG. 5-3. Computer Model of Drag Coefficient for Double Parabolic Airfoil in Transonic Flow (based on ref. [*55*])

proportion to $M_t^2/(1-M_t)$. (ii) The far field loading noise is proportional to $M_t/(1-M_t)^2$, whereas the near field loading noise is to $1/(1-M_t)$ when the total loading value is fixed. (iii) When the collective pitch angle is given, the loading noise should be multiplied by M_t^2.

These results are also shown in Table 5-1.

Fig. 5-2 shows the variation of calculated results of peak-to-peak amplitude of acoustic pressure in each noise component vs. tip Mach number M_t keeping the total torque constant. For a subsonic tip speed rotor, each noise component increases its level with the increase of tip speed, and above all the thickness noise has the maximum increasing rate. This character can be predicted by the former dimensional analysis. But in the case of a supersonic rotor, it is shown in Fig. 5-2 that a maximum value exists in the far field noise containing thickness noise. This maximum of noise level in the change of rotational speed exists even by taking the effect of tansonic drag divergence shown in Fig. 5-3 [55] into the calculation as is shown in Fig. 5-4.

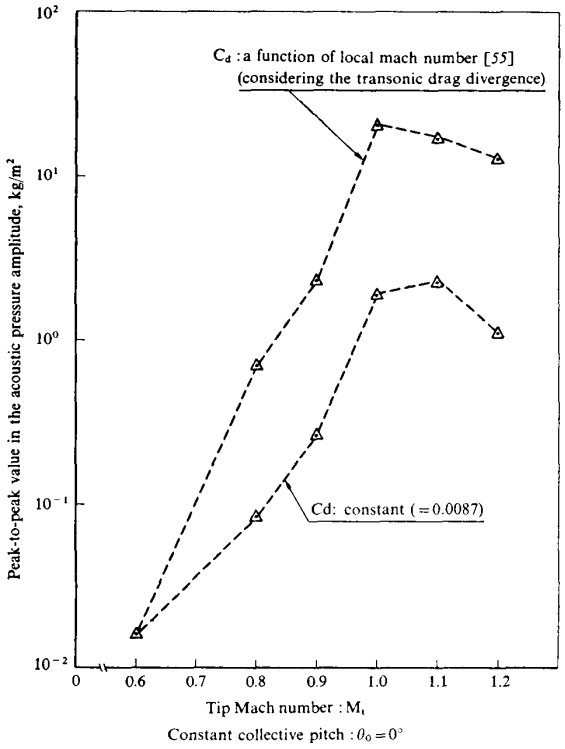

FIG. 5-4. Variation of the Peak-to-Peak Value in the Acoustic Pressure Amplitude vs. Tip Mach Number for the Rotor (A) Taking into Account the Transonic Drag Divergence

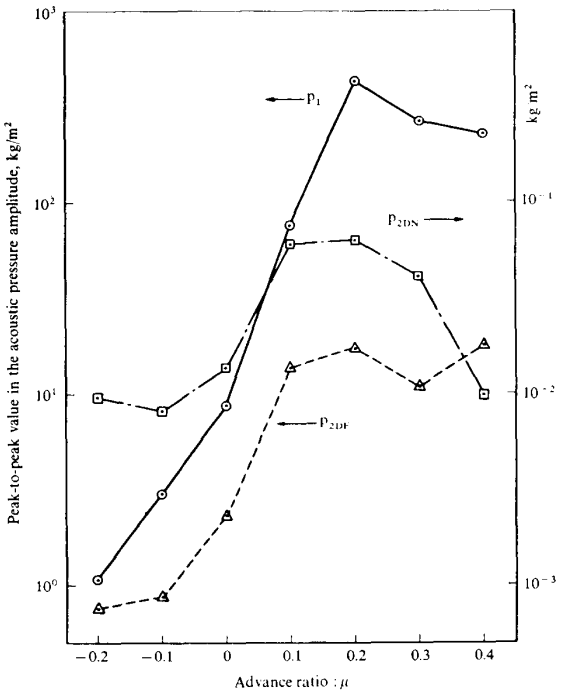

FIG. 5-5. Variation of Peak-to-Peak Value in the Acoustic Pressure Amplitude vs. Advance Ratio for the Rotor (A)

5-2 *Advance Ratio*

Fig. 5-5 shows the variation of peak-to-peak value of each noise component vs. advance ratio μ (nondimentionalized forward speed by a rotational speed), keeping the total thrust and torque constant. Here, the negative advance ratio means that of a leaving rotor, whereas the positive value means that of an approaching rotor towards the observer. The zero advance ratio indicates that of a hovering rotor.

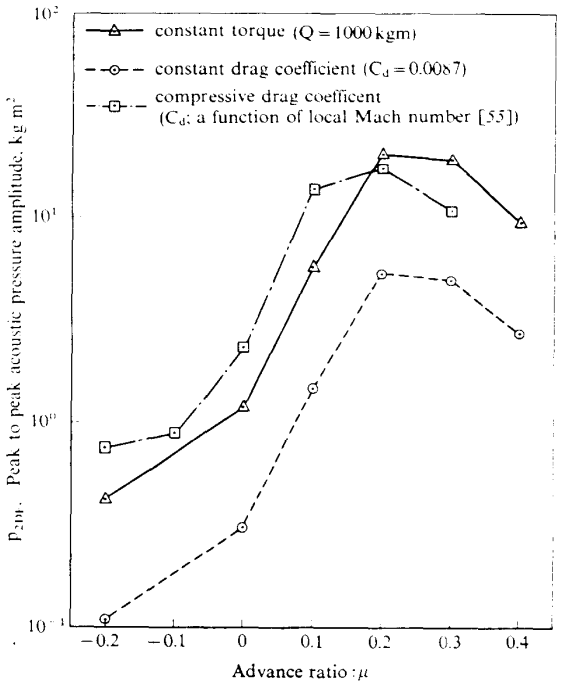

FIG. 5-6. Variation of Peak-to-Peak Acoustic Pressure Amplitude vs. Advance Ratio for the Rotor (A)

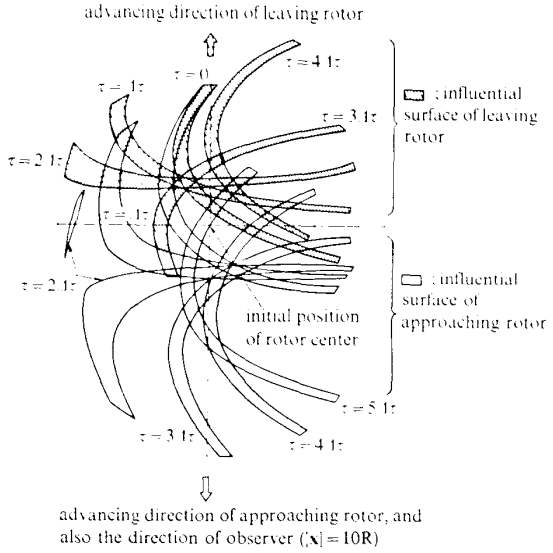

FIG. 5-7. Difference of Deformation of Influential Surfaces between Approaching Rotor and Leaving Rotor ($\mu = \pm 0.2$, $M_t = 0.9$; $\Delta t = 1$ period/6)

The acoustic level increases rapidly with the increase of advance ratio in $\mu \leq 0.2$. Then it decreases with μ. This tendency is still kept in the case considering the transonic drag divergence as shown in Fig. 5-6.

The area of influential surface of approaching rotor is geater than that of leaving one (Fig. 5-7). However, when the approaching speed is faster than the speed of sound which is the contracting rate of acoustic sphere, the elongation of the influential surface no longer increases, but begins to decrease with advance ratio. The results of Fig. 5-6 may be explained clearly by this concept based on the elongation or the contraction of the area of influential surface.

5-3 Number of Blades

Fig. 5-8 shows the variation of peak-to-peak value of each noise component vs. number of blades, keeping the total torque and chord length constant. Then, as the blade number increases, the wing loading decreases, and so does the acoustic level.

This result is brought by the degree of the local elongation of the influential surface. The maximum rate of deformaion of influential surface is observed at $\psi = 90°$ in the blade tip region. This local elongation effect may be attenuated by the increase of blade number.

5-4 Chord Length

Fig. 5-9 shows the variation of peak-to-peak value of each noise component vs. chord length, keeping the total torque constant. As the chord length increases the wing loading decreases, and so does slightly the acoustic level.

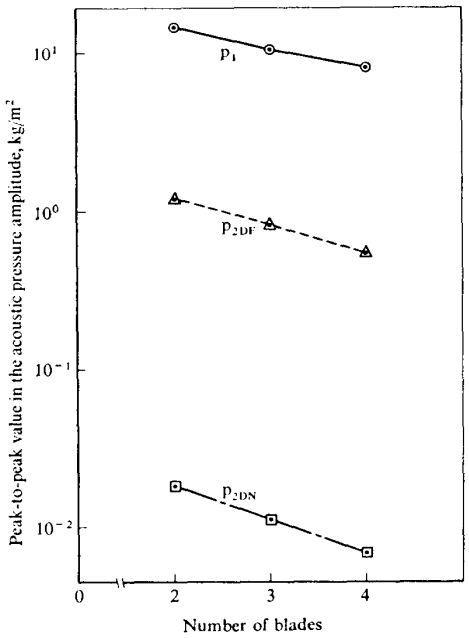

FIG. 5-8. Variation of the Peak-to-Peak Values in the Acoustic Pressure Amplitude vs. Number of Blades for the Rotor (A)

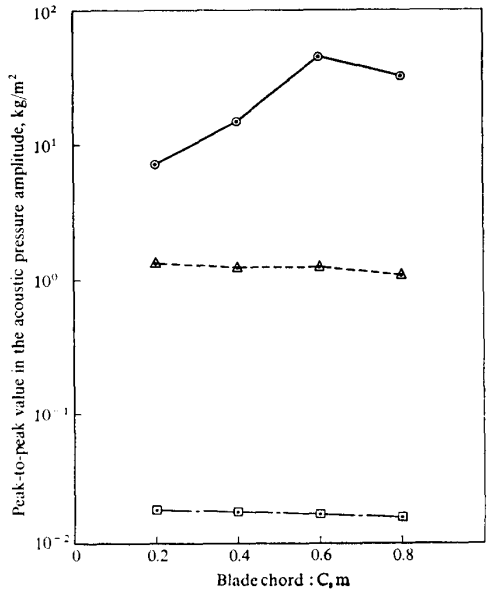

FIG. 5-9. Variation of the Peak-to-Peak Value in the Acoustic Pressure Amplitude vs. Chord Length for the Rotor (A)

This result is also explained by the attenuation effect due to the local elongation of the influential surface, but is not so big as the former case in 5-3.

In the case of thickness noise, however, the area of distributed noise source is proportional to the chord length, and thus the thickness noise increases with the increase of chord length. Coupled with the attenuation effect of the local elongation of influential surface, the thickness noise has a maximum value at an appropriate chord length.

5-5 Rotor Diameter

The thrust is proportional to disk area multiplied by square of the rotor tip speed. It will, then, be appreciated that the larger disk area has smaller noise level for a given pay-load and that the helicopter is considered to be the most quiet flying vehicle among all of VTOL aircraft.

Fig. 5–10 shows the variation of peak-to-peak value of each noise component vs. rotor radius, keeping the similarity of a rotor geometry, total thrust, total torque, and tip speed constant.

The source strength of thickness noise is equal for any rotor having similar geometry (thickness ratio and shape of airfoil section) and tip speed, where the area of influential surface is proportional to R^2. The source strength of thrust noise doesn't vary with rotor radius for a given thrust, whereas that of drag noise is proportional to R^{-1} for a given torque.

On the other hand, the shape of influential surface can be considered to be unchanged for the observer located in sufficiently far field compared with the rotor radius. For the far field noise, the differentiation with respect to time will have an effect being proportional to the rotational speed Ω, that is to say to R^{-1} for a given tip speed rotor.

In conclusion, it may be said that the thickness noise is proportional to R, the near

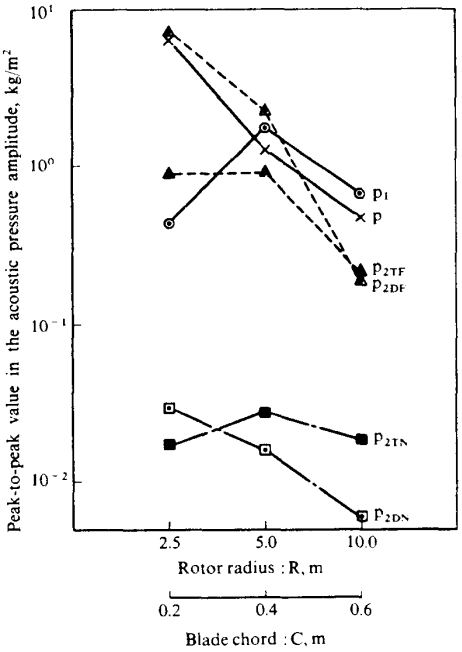

FIG. 5-10. Variation of the Peak-to-Peak Value in the Acoustic Pressure Amplitude vs. Blade Dimension for the Rotor (A) (blade aspect ratio is 12.5)

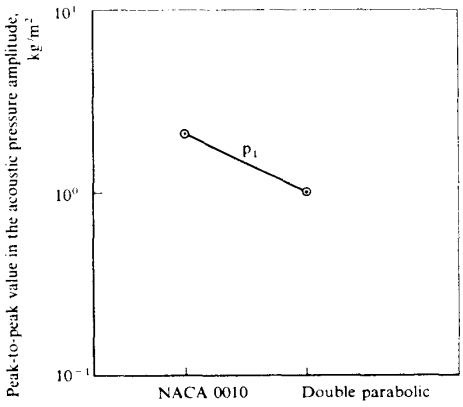

FIG. 5-11. Thickness Noise vs. Airfoil Section Shape for the Rotor (A)

field thrust noise R^0, the far field thrust noise R^{-1}, the near field drag noise R^{-1}, the far field drag noise R^{-2}, respectively. This is the analytic explanation for Fig. 5-10.

5-6 Airfoil Section and Load Distribution

1) Airfoil Section

Fig. 5-11 shows the peak-to-peak value of thickness noise for two kinds of airfoil section, keeping the thickness ratio and the chord length constant. One of them is NACA 4-digit airfoil (NACA 0010), and the other is double parabolic airfoil. The noise level of the former is a little higher than that of the latter.

Since the sound pressure depends on both the source strength which is proportional to the change of thickness along the chord, $\partial h/\partial \eta_1$, and the deformation of the influential surface, it is necessary for reducing the noise level to make a uniform distribution of $\partial h/\partial \eta_1$ in a given chord. The NACA 4-digit airfoil has a infinite value of $\partial h/\partial \eta_1$ at leading edge as was shown in Fig. 3-1, whereas the double parabolic airfoil has a linear distribution of $\partial h/\partial \eta_1$ along the chord.

2) Load Distribution

a) Chordwise Distribution—Fig. 5-12 shows the peak-to-peak value of the far field thrust noise for some kinds of chordwise load distibution such as rectangular, saw tooth, and saw tooth 10% from leading edge, keeping the total thrust and the total torque constant. Like the thickness noise the more the load distribution is concentrated, the higher noise is produced.

The case of a pillar model which is a concentrated load model in both chordwise directions is also shown in this figure. Its noise level is higher than the other distribution models.

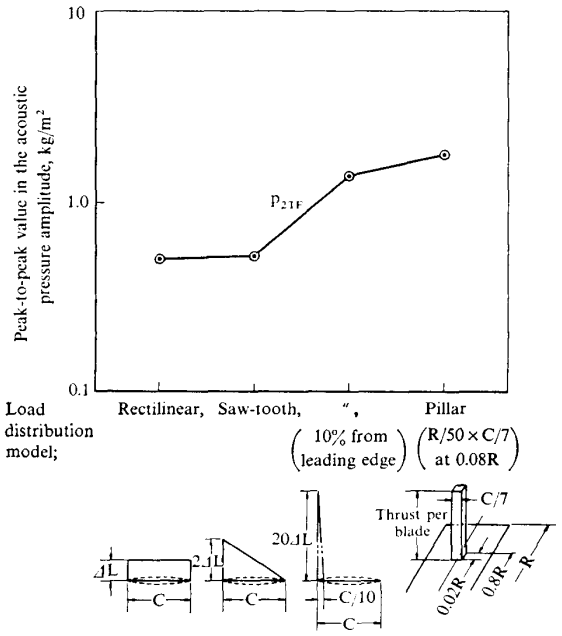

FIG. 5-12. Variation of Peak-to-Peak Value in the Acoustic Pressure Amplitude vs. Chordwise Load Distribution (total loading value is equalized for each case) for the rotor (A)

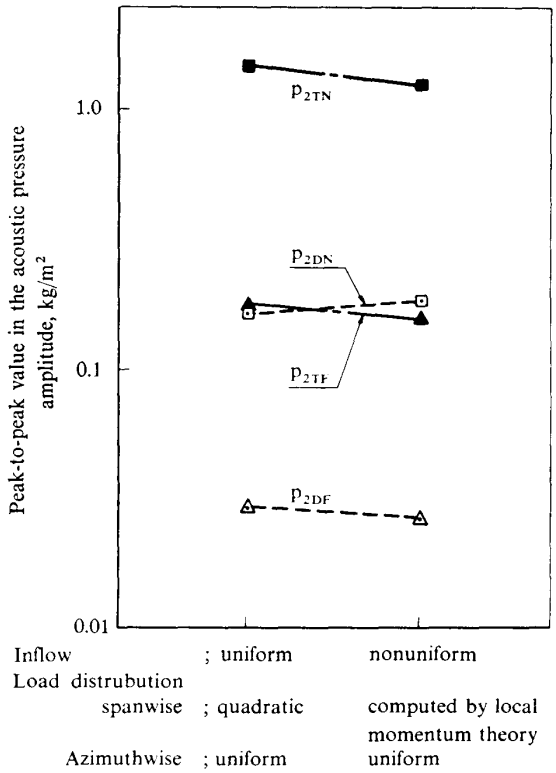

FIG. 5-13. Variation of Peak-to-Peak Value in the Acoustic Pressure Amplitude vs. Disc Load Distribution for the Rotor (B)

b) Azimuthal Distribution—Fig. 5-13 shows the peak-to-peak value of the loading noise for two kinds of load distribution model, keeping the total thrust and the total torque constant.

One example is a simple model assuming a uniform inflow (chordwise; rectangular, spanwise; quadratic, and azimuthal; uniform) which is adopted in almost every case in this report, and the other is a precisely calculated model considering a nonuniform inflow by the local momentum theory [*56*]. In the latter model the lift and drag can be computed for an arbitrary flight condition with the following mesh size; one twentieth of rotor radius in spanwise and every ten degrees in azimuthal directions. The computed load distribution used in the calculation of noise level given by Fig. 5-13 is shown in Fig. 5-14 (a), (b), where the chordwise load distribution is assumed to be rectangular.

In Fig. 5–13, the difference in noise level between two models is not so large that the simplified load distribution can be adopted for the calculation of noise level of other examples in this paper. It must be noticed that the allowable mesh dimension in the present calculation by using the computer, FACOM 230/75, ISAS, University of Tokyo, is so large that the effect of blade-vortex interaction, which has been said to be a important cause of blade slap, can not be predictable.

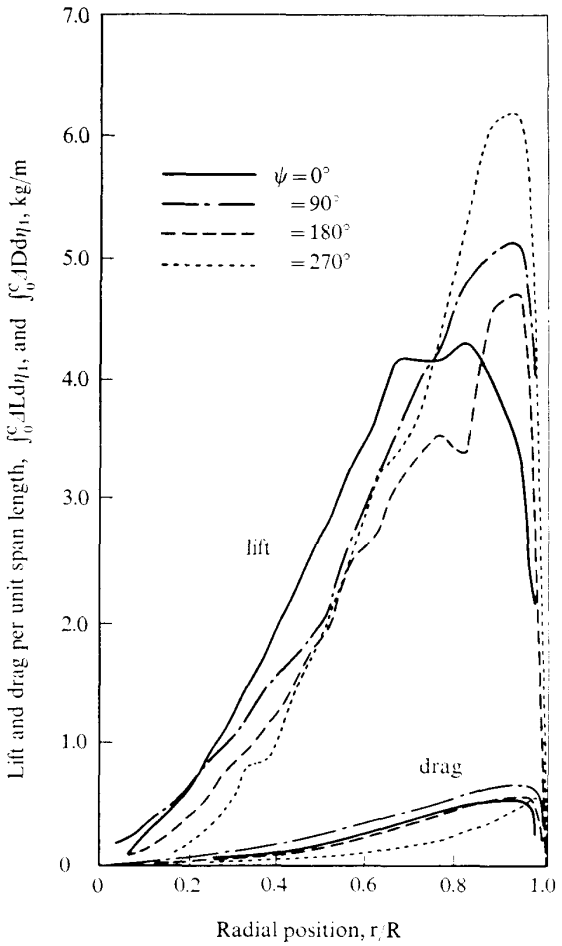

FIG. 5-14 (a). Load Distribution by Local Momentum theory [*56*] for the Rotor (B) (mesh size; $\Delta R = R/20$)

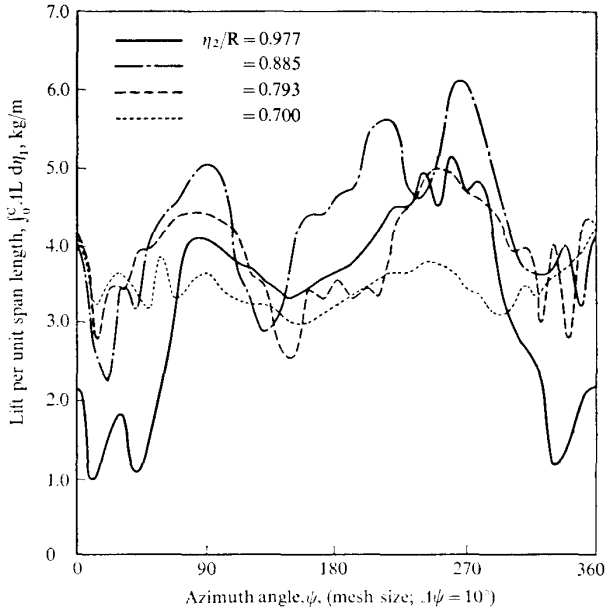

FIG. 5-14 (b). Load Distribution by Local Momentum Theory [*56*] for the Rotor (B)

5-7 Directivity

1) Vertical Directivity

Fig. 5-15 shows the variation of peak-to-peak value of each noise component for hovering rotor vs. observer elevation angle to the rotor plane, δ, keeping the distance from the rotor hub center constant. The same result is shown in Fig. 5-16 by polar graph.

The thickness noise (monopole; isotropic) and the drag noise (longitudinal dipole) propagate most strongly to the direction of rotor plane ($\delta=0°$), whereas the thrust noise (lateral dipole) doesn't propagate in the rotor plane as explained before. All noise components don't propagate to the direction of rotor axis where the change of deformation of influential surface cannot be observed.

It must, however, be noticed that the rotor having a nonuniform azimuthal lift distribution radiates the thrust noise to the direction of rotor axis, but not other components. Hence, the azimuthal spectrum of the load distribution can be obtained from the harmonic analysis of noise measured on the rotor axis [*57*].

2) Horizontal Directivity

Fig. 5-17 shows the variation of peak-to-peak value of each noise component for a

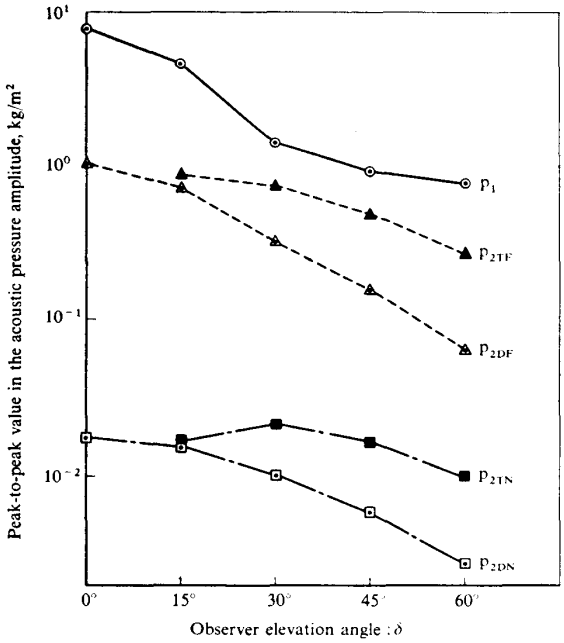

FIG. 5-15. Variation of the Peak-to-Peak Value in the Acoustic Pressure Amplitude vs. Observer Elevation Angle for the Rotor (A)

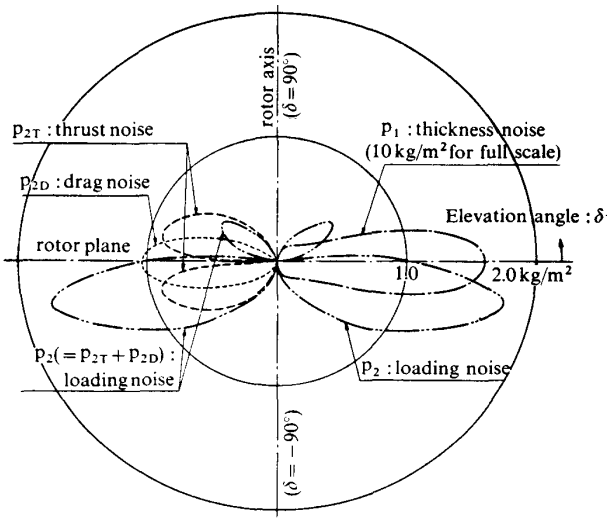

FIG. 5-16. Directivity of each Component of Acoustic Pressure for the Rotor (A)

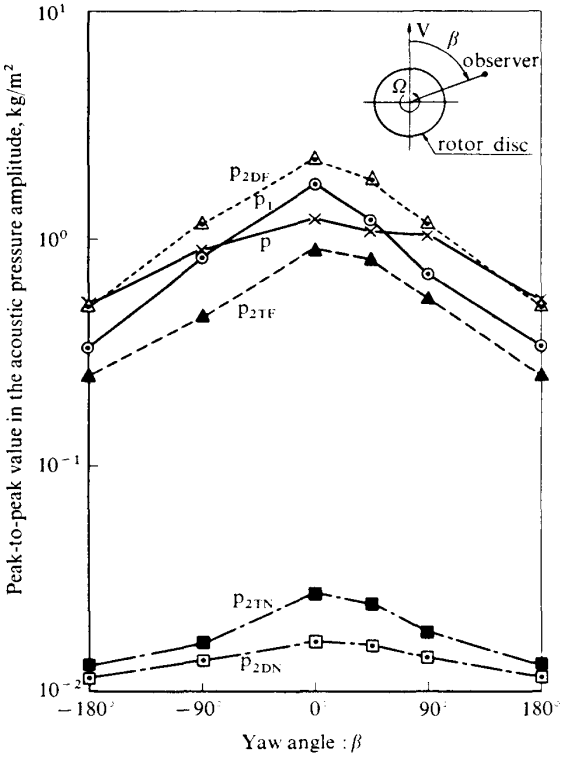

FIG. 5-17. Directivity of Each Component in Forward Flight (μ=0.2) for the Rotor (A)

rotor in forward flight vs. observer yaw angle β, keeping the distance from the rotor hub center constant.

There exists a non-symmetry of horizontal directivity based on the rotating direc-

tion. The advancing blade side has a greater noise source than the retreating side, then a little bigger noise will be observed in this side.

As an example of this result, it is recommended to fly the helicopter on a route such that in order to reduce the noise level hospitals and schools must be located in the blade retreating side.

6. Conclusion

By decomposing the noise sources into five components such as thickness noise, near field thrust noise, far field thrust noise, near field drag noise, and far field drag noise, and by separating the solution of wave equation into integrand and integral region, it was made possible to predict "analytically" the characteristics of acoustic field. The characteristics of acoustic pressure such as wave form, peak-to-peak value, directivity, spectrum, etc . . . are functions of the following various parameters: rotor geometry such as rotor diameter, number of blades, chord length, blade planform, shape of airfoil section, and so on, and operating conditions such as rotor rotational speed, advance ratio, maneuvering parameters, observer motion and/or position, and so on. The analytical predictions were assured by the precise computer calculation in wide range.

Throughout these calculations, the thickness noise was proved to be a sufficiently predominant, specifically for high tip speed rotor. This may be, thus, considered to be one of suspective causes of "slap" though it is believed to occur by the blade-vortex interaction [*15–19*].

Through these parametric analyses, the following way of noise reduction may be proposed: (i) rotate a large rotor slowly, (ii) increase the number of blades, (iii) reduce the concentration of source strength, (iv) decrease a blade thickness ratio, (v) attenuate the strength of blade tip vortex, (vi) find a flight pass to minimize the noise for a given observer position by considering its directivity.

Typical examples of computed results were compared with both the experimental results and some of the previous harmonic theories. The agreement with the experimental results is in a good degree. Though the simple harmonic theory which neglects the thickness noise and assumes a rotating point force didn't agree well with the present theory, the advanced harmonic theory based on the distributed sources model coincided fairly well with the present theory. These coincidence are considered to guarantee the accuracy of the present theory.

The blade-vortex-interaction noise which has been said to be a suspective cause of blade slap was not able to be computed in a satisfactory manner because of the capacity of computer. In order to account this interaction effect, the mesh size for a numerical integration should be sufficiently fine compared with the radius of tip vortex core which may have the order of one tenth of a chord length. This effect was investigated by the author in some extent [*59*], and the experimental results showed the strong correlation between the blade-vortex-interaction and the impulsive noise.

Acknowledgements

The author is indebted to Professor A. Azuma, University of Tokyo, for his valuable

advices and encouragement during this work.

The numerical calculations were carried out on the computer FACOM230/75 at the Data Processing Center, Institute of Space and Aeronautical Science, University of Tokyo.

Department of Aerodynamics
Institute of Space and Aeronautical Science
University of Tokyo, Tokyo
June 25, 1977

Appendix A. Solution of Wave Equation Using the Influential Surface Method

For a body in motion, whose surface is described by $f(\boldsymbol{y}, \tau)=0$, the equation for determing the acoustic pressure p was given by Ffowcs Williams and Hawkings as [*5*1]:

$$\Box p = \frac{\partial}{\partial \tau}[\rho_0 v_n |\nabla f| \delta(f)] - \frac{\partial}{\partial y_i}\left[P_{ij}\frac{\partial f}{\partial y_j}\delta(f)\right] + \frac{\partial^2}{\partial y_i \partial y_j} T_{ij} \tag{A1}$$

where $\Box\left(=\frac{1}{c^2}\frac{\partial^2}{\partial \tau^2} - \nabla^2\right)$ is a wave operator.

The first term in the above equation arises as a result of the motion of the surface in the normal direction. The second term comes from the local surface stress tensor P_{ij} which consists of viscous stress and the thermodynamic pressure. The third term is the so-called quadrupole noise due to turbulence as was derived by Lighthill in his jet noise theory [*3–5*].

Since in the cases of rotor or fan blade, the region of turbulent flow is small and its intensity is relatively low, the turbulence is very inefficient in producing the noise. Therefore, the term involving T_{ij} and the viscous effect in P_{ij} may be neglected in the wave equation.

Under the above assumptions the equation governing the generation of the sound pressure for moving bodies is;

$$\Box p = \frac{\partial}{\partial \tau}[\rho_0 v_n |\nabla f| \delta(f)] - \frac{\partial}{\partial y_i}\left[p_b \frac{\partial f}{\partial y_j}\delta(f)\right] \tag{A2}$$

where p_b is the body surface pressure.

In the right hand side of the equality, the first term is the thickness noise source, and the second term is the loading noise source, respectively.

In the solution of this equation, the geometry and the time history of the motion of the body will be assumed as known.

Consider the wave equation of arbitrary source $A(\boldsymbol{y}, \tau)$ as:

$$\Box p = A(\boldsymbol{y}, \tau)|\nabla f|\delta(f) \tag{A3}$$

where ∇f means outward normal vector to the body surface and $\delta(\ )$ is a Dirac's delta function. A general expression of source, $A(\boldsymbol{y}, \tau)$, will be used here to represent the

actual source such as thickness noise source or loading noise source.

The Green's function for the wave equation in free field is denoted by

$$G(r, t) = \delta(g)/4\pi r \tag{A4}$$

$$g = \tau - t + \frac{r}{c} \ (=0;\ \text{acoustic sphere}) \tag{A5}$$

where $r=|\boldsymbol{x}-\boldsymbol{y}|$, and $\boldsymbol{x}$ and $\boldsymbol{y}$ are position vectors of the observer and the source respectively, and where t and τ are time of the observer and the source respectively.

Then the solution of equation (A3) will be given by using Green's function as follows:

$$p(\boldsymbol{x}, t) = \frac{1}{4\pi}\int\int \frac{A(\boldsymbol{y}, \tau)}{r} |\nabla f|\delta(f)\delta(g)d\boldsymbol{y}d\tau\ , \tag{A6}$$

where $\int d\boldsymbol{y}$ is a volume integration all over the space, and $\int d\tau$ is a source time integration for the interval of $-\infty<\tau\leq t$.

The integrations containing delta function have been studied in the field of "generalized function" in mathematics [*60*, *61*].

It is, anyway, shown by equation (A6) that the solution is given by the integration on the locus of contracting sphere $g(\tau; \boldsymbol{x}, t)=0$ and the moving body surface $f(\boldsymbol{y}, \tau)=0$.

This locus for a given observer time and position is named here as "influential surface", because all signals on this surface will arrive simultaneously to the observer position $\boldsymbol{x}$, at time t. This influential surface is shown in Fig. 2-3 as Σ surface.

Integrating variable in equation (A6) $d\boldsymbol{y}$ can be transformed as follows:

$$\begin{aligned} d\boldsymbol{y} = dy_1dy_2dy_3 &= dy_1dfdg \Big/ \frac{\partial(y_1, f, g)}{\partial(y_1, y_2, y_3)} = dy_1dfdg \Big/ \frac{\partial(f, g)}{\partial(y_2, y_3)} \\ &= dy_1dfdg \Bigg/ \begin{vmatrix} \dfrac{\partial f}{\partial y_2}, & \dfrac{\partial f}{\partial y_3} \\ \dfrac{\partial g}{\partial y_2}, & \dfrac{\partial g}{\partial y_3} \end{vmatrix} \\ &= dy_1dfdg/(\nabla f \times \nabla g)\cdot \boldsymbol{e}_1 \\ &= dy_1dfdg/|\nabla f||\nabla g|(\boldsymbol{n} \times \hat{\boldsymbol{r}})\cdot \boldsymbol{e}_1 \\ &= cdy_1dfdg/|\nabla f| \sin\theta \cos\theta_1 \\ &= cdfdgd\Gamma/|\nabla f| \sin\theta \end{aligned} \tag{A7}$$

because,

$$|\nabla g| = \left|\frac{1}{c}\ \frac{\boldsymbol{r}}{r}\right| = \frac{1}{c}$$

and

$$dy_1 = d\Gamma \cos\theta_1$$

where

$\boldsymbol{e}_1$: unit vector along y_1 axis

Γ: intersecting line of $f=0$ and $g=0$

$\boldsymbol{n}$: $\left(=\dfrac{\nabla f}{|\nabla f|}\right)$ unit vector outward normal to body surface

$\boldsymbol{f}$: $\left(=\dfrac{\nabla g}{|\nabla g|}\right)$ unit vector in radiation direction

θ: angle between $\boldsymbol{n}$ and $\hat{\boldsymbol{r}}$

θ_1: angle between Γ and $\boldsymbol{e}_1$.

With this transformation, equation (A4) becomes:

$$p(\boldsymbol{x}, t)=\frac{1}{4\pi}\int_{\tau_1}^{\tau_2}\int_{\Gamma}\frac{cA(\boldsymbol{y}, \tau)}{r\sin\theta}d\Gamma d\tau \tag{A8}$$

where τ_1 and τ_2 are the source times at which acoustic sphere, $g=0$, enters and leaves the body.

Next, the solution of the following equations will be studied.

$$\Box p_1=\frac{\partial}{\partial\tau}[A(\boldsymbol{y}, \tau)|\nabla f|\delta(f)] \tag{A9}$$

$$\Box p_2=\frac{\partial}{\partial y_i}[A_i(\boldsymbol{y}, \tau)|\nabla f|\delta(f)] \tag{A10}$$

Since the operator $\Box$ commutes with oprators $\partial/\partial\tau$ and $\partial/\partial y_i$, from equation (A8), it follows that

$$4\pi p_1(\boldsymbol{x}, t)=\frac{\partial}{\partial t}\int_{\tau_1}^{\tau_2}\int_{\Gamma}\frac{cA(\boldsymbol{y}, \tau)}{r\sin\theta}d\Gamma d\tau \tag{A11}$$

$$4\pi p_2(\boldsymbol{x}, t)=\frac{\partial}{\partial x_i}\int_{\tau_1}^{\tau_2}\int_{\Gamma}\frac{cA_i(\boldsymbol{y}, \tau)}{r\sin\theta}d\Gamma d\tau\,. \tag{A12}$$

By using the following relation:

$$\frac{\partial}{\partial x_i}[\ ]_{ret}=\left[\frac{\partial}{\partial x_i}+\frac{\partial\tau}{\partial x_i}\frac{\partial}{\partial\tau}\right]_{ret}=\left[\frac{\partial}{\partial x_i}-\frac{1}{c}\frac{r_i}{r}\frac{\partial}{\partial\tau}\right]_{ret} \tag{A13}$$

where

$$r_i=|x_i-y_i|\,,$$

equation (A12) can be rewritten as:

$$\begin{aligned}4\pi p_2(\boldsymbol{x}, t)&=\int_{\tau_1}^{\tau_2}\int_{\Gamma}\left\{\frac{\partial}{\partial x_i}\frac{cA_i(\boldsymbol{y}, \tau)}{r\sin\theta}-\frac{r_i}{r}\frac{\partial}{\partial t}\frac{A_i(\boldsymbol{y}, \tau)}{r\sin\theta}\right\}d\Gamma d\tau\\&=-\int_{\tau_1}^{\tau_2}\int_{\Gamma}\frac{cA_r(\boldsymbol{y}, \tau)}{r^2\sin\theta}d\Gamma d\tau-\frac{\partial}{\partial t}\int_{\tau_1}^{\tau_2}\int_{\Gamma}\frac{A_r(\boldsymbol{y}, \tau)}{r\sin\theta}d\Gamma d\tau\end{aligned} \tag{A14}$$

where

$$A_r(\boldsymbol{y}, \tau)=A_i(\boldsymbol{y}, \tau)r_i/r$$

The importance of this result lies in the fact that now only one derivative, that is, the time derivative, appears in the solution which may be performed numerically for a fixed observer position. This is considerably simpler than using equation (A12) in which the space derivatives must be calculated numerically at a fixed observer time.

When the relation of equations (A11), and (A14) are used, the following solutions of the wave equation (A2) are obtained for thickness source and loading source respectively:

$$4\pi p_1(\boldsymbol{x}, t) = \frac{\partial}{\partial t}\int_{\tau_1}^{\tau_2}\int_{\Gamma}\frac{\rho_0 c v_n}{r\sin\theta}\,d\Gamma d\tau \tag{A15}$$

$$4\pi p_2(\boldsymbol{x}, t) = \int_{\tau_1}^{\tau_2}\int_{\Gamma}\frac{cp_b\cot\theta}{r^2}\,d\Gamma d\tau + \frac{\partial}{\partial t}\int_{\tau_1}^{\tau_2}\int_{\Gamma}\frac{p_b\cot\theta}{r}\,d\Gamma d\tau \tag{A16}$$

Appendix B. Application to Helicopter Rotor

Two coordinate systems are used as shown in Fig. 2-1, in which the $\boldsymbol{\eta}$-frame is fixed to the blade such that the η_1-axis is parallel to the chord, η_2-axis is along the span, η_3-axis is along the rotor axis and the $\boldsymbol{y}$-frame is fixed to the undisturbed fluid. The position vector of the origin of the $\boldsymbol{\eta}$-frame is $\boldsymbol{y}_H(\tau)$ and the angle between η_1-axis and y_1 axis is ϕ.

Let $\eta_3 = h(\eta_1, \eta_2)$ be the equation of the thickness distribution. For a camberless airfoil, the equation of the surface of the blade in the $\boldsymbol{\eta}$-frame is:

$$f_\eta(\boldsymbol{\eta}) = \eta_3 \mp h(\eta_1, \eta_2) = 0 \tag{B1}$$

where negative and positive sign correspond to the upper and lower surfaces of the blade respectively. This equation is written in such a way that $f_\eta(\boldsymbol{\eta})<0$ shows inside the blade and $f_\eta(\boldsymbol{\eta})>0$ shows outside the blade.

The equation of the blade surface in the $\boldsymbol{y}$-frame, $f(\boldsymbol{y}, \tau)=0$, is obtained by the following relation about the coordinate transformation:

$$f(\boldsymbol{y}, \tau) = f_\eta[\boldsymbol{\eta}(\boldsymbol{y}, \tau)] = 0 \tag{B2}$$

$$\left.\begin{aligned}
\eta_1 &= (y_1 - y_{H1})\cos\phi + (y_2 - y_{H2})\sin\phi \\
\eta_2 &= -(y_1 - y_{H1})\sin\phi + (y_2 - y_{H2})\cos\phi \\
\eta_3 &= y_3 - y_{H3}
\end{aligned}\right\} \tag{B3}$$

The normal velocity v_n of the surface is found from the relation,

$$v_n = -\frac{\partial f/\partial\tau}{|\nabla f|}\,. \tag{B4}$$

From equation (B2), the following relations are obtained:

$$\frac{\partial f}{\partial\tau} = \frac{\partial h}{\partial\eta_1}(V_{\eta_1} - \eta_2\Omega) + \frac{\partial h}{\partial\eta_2}(V_{\eta_2} + \eta_1\Omega) \mp V_{\eta_3} \tag{B5}$$

$$|\nabla f|^2 = 1 + \left(\frac{\partial h}{\partial\eta_1}\right)^2 + \left(\frac{\partial h}{\partial\eta_2}\right)^2 \tag{B6}$$

$$\nabla f \cdot \hat{\boldsymbol{r}} = |\nabla f| \cos\theta = -\frac{\partial h}{\partial \eta_1}\hat{r}_1 - \frac{\partial h}{\partial \eta_2}\hat{r}_2 \pm \hat{r}_3 \tag{B7}$$

where $(V_{\eta_1}, V_{\eta_2}, V_{\eta_3})$ are the components of the vehicle velocity $\boldsymbol{V}$ in the $\boldsymbol{\eta}$-frame, Ω is the angular velocity of the rotor, and $(\hat{r}_1, \hat{r}_2, \hat{r}_2)$ are the components of the unit radiation vector $\hat{\boldsymbol{r}}$ in the η-frame.

Combining equations (B6), (B7) under the assumption of $\partial h/\partial \eta_2 \ll 1$ yields:

$$|\nabla f|^2 \sin^2\theta = 1 - \hat{r}_3^2 + \left(\frac{\partial h}{\partial \eta_1}\right)^2 (1 - \hat{r}_1^2) \equiv \lambda^2 \tag{B8}$$

Substituting equations (B4), (B5), and (B8) into the solution of thickness noise (A15) yields:

$$p_1(\boldsymbol{x}, t) = \frac{\rho_0 c}{2\pi}\frac{\partial}{\partial t}\int_{\tau_1}^{\tau_2}\int_{\Gamma} \frac{(\partial h/\partial \eta_1)(-V_{\eta_1} + \eta_2 \Omega)}{r\lambda} d\Gamma d\tau \tag{B9}$$

When equations (B7) and (B8) are used, the solution of loading noise (A16) is obtained as follows:

$$p_2(\boldsymbol{x}, t) = -\frac{\partial}{\partial t}\int_{\tau_1}^{\tau_2}\int_{\Gamma} k(\boldsymbol{\eta}, \tau) d\Gamma d\tau - c\int_{\tau_2}^{\tau_1}\int_{\Gamma} \frac{k(\boldsymbol{\eta}, \tau)}{r} d\Gamma d\tau \tag{B10}$$

where

$$k(\boldsymbol{\eta}, \tau) = \frac{-(p_U - p_L)\hat{r}_3 + (p_U + p_L)\partial h/\partial \eta_1 \hat{r}_1}{4\pi r\lambda} \tag{B11}$$

and where p_U and p_L are the pressure of upper and lower surface of the blade respectively.

The relations between p_L, p_U and ΔL, ΔD, is as follows:

$$\Delta L = (p_L - p_U)\cos\alpha = (p_L - p_U)/\sqrt{1 + (\partial h/\partial \eta_1)^2} \tag{B12}$$

$$\Delta D = (p_L + p_U)\sin\alpha = (p_L + p_U)\frac{\partial h}{\partial \eta_1}\Big/\sqrt{1 + (\partial h/\partial \eta_1)^2} \tag{B13}$$

where $\alpha \equiv \tan^{-1}(\partial h/\partial \eta_1)$. With these relations, equation (B11) can be rewritten as:

$$k(\boldsymbol{\eta}, \tau) = \frac{-\Delta L \cdot \hat{r}_3 + \Delta D \cdot \hat{r}_1 \cdot \sqrt{1 + (\partial h/\partial \eta_1)^2}}{4\pi r\lambda} \tag{B14}$$

The acoustic pressure from each blade must be added linearly in equations (B9) and (B10) to get a instantaneous pressure for a given observer time. The successive computation of this pressure with a little change of time gives an acoustic wave form for a given observer position.

References

[1] Igarashi, Juichi: Problems of Aircraft Noise, Journal of the Acoustical Society of Japan, Vol. 26, No. 6, 1970, in Japanese.

[2] Nagasawa, Osamu: On the Certification of Aircraft Noise, Journal of the Japan Society for Aeronautical and Space Sciences, Vol. 20, No. 216, 1971/1, in Japanese.

[3] Lighthill, M. J.: On Sound Generated Aerodynamically. I. General Theory, Proceedings of

Royal Society, A 211, pp. 564–587.
[4] Lighthill, M. J.: On Sound Generated Aerodynamically. II. Turbulence as a Source of Sound, Proceedings of Royal Society, A 222, 1954, pp. 1–32.
[5] Lighthill, M. J.: Jet Noise, AIAA Journal, Vol. 1, No. 7, 1963, pp. 1507–1517.
[6] Kotake, Susumu: Jet Noise, Journal of the Japan Society for Aeronautics and Space Sciences, Vol. 11, No. 113, 1963/6, in Japanese.
[7] Kotake, Susumu and Okazaki, Takuro: Jet Noise, Journal of the Japan Society for Mechanical Engineerings, Vol. 67, No. 547, 1964/8, in Japanese.
[8] Kaji, Shojiro and Okazaki, Takuro: Axial Compressor Noise, Journal of the Japan Society for Mechanical Engineerings, Vol. 70, No. 581, 1976/6, in Japanese.
[9] Kaji, Shojiro and Okazaki, Takuro: Rotational Noise of Axial Compressor Journal of the Japan Society for Aeronautics and Space Science, Vol. 18, No. 192 1970/1, in Japanese.
[10] Kaji, Shojiro and Okazaki, Takuro: Aircraft Engine Noise, Journal of the Japan Society for Aeronautics and Space Sciences, Vol. 21, No. 230, 1973/3, in Japanese.
[11] Nisinomiya, Guén: Helicopter Noise, Journal of the Acoustical Sciety of Japan, Vol. 32, No. 8, 1976/8, in Japanese.
[12] Azuma, Akira: Helicopter Noise, Journal of the Japan Society for Aeronautical and Space Sciences, Vol. 23, No. 254, 1973/3, in Japanese.
[13] Stepniewski, W. Z. and Schmitz, F. H.: Possibilities and Problems of Achieving Community Noise Acceptance of VTOL, Aeronautical Journal, June, 1973.
[14] Munch, Charles L.: A Study of Noise Guidelines for Community Acceptance of Civil Helicopter Operations, Journal of the American Helicopter Society, Vol. 20, No. 1, January, 1975.
[15] Leverton, John W. and Taylor, F. W.: Helicopter Blade Slap, Journal of Sound and Vibration, Vol. 4, No. 3, 1966, pp. 345–357.
[16] Leverton John W.: Helicopter Noise Blade Slap. Part 1: Review and Theoretical Study, NASA CR–1221, 1968.
[17] Leverton, John W.: Helicopter Noise Blade Slap. Part 2: Experimental Results, NASA CR–1983, 1972.
[18] Widnall, Sheila E.: Helicopter Noise Due to Blade-Vortex Interaction, The Journal of the Acoustical Society of America, Vol. 50, No. 1 (part 2), 1971, pp. 354–365.
[19] Filotas, L. T.: Vortex Induced Helicopter Blade Loads and Noise, Journal of Sound and Vibration, Vol. 27, No. 3, 1973, pp. 387–398.
[20] Lyon, R. H.: Radiation of Sound by Airfoils that Accelerate Near the Speed of Sound, The Journal of the Acoustical Society of America, Vol. 49, No. 3 (part 2), 1971, pp. 894–905.
[21] Farassat, F.: Theory of Noise Generation from Moving Bodies with an Application to Helicopter Rotors, NASA TR R–451, 1975/12.
[22] Farassat, F., Pegg, R. J. and Hilton, D. A.: Thickness Noise of Helicopter Rotors at High Tip Speeds, 2nd AIAA Aero-Acoustics Conference, AIAA paper 75–453, 1975/3.
[23] Farassat, F. and Brown, T. J.: Development of a Noncompact Source Theory with Application to Helicopter Rotors, 3rd AIAA Aero-Acoustics Conference, AIAA paper 76–563, 1976/7.
[24] Hanson D. B.: Near Field Noise of High Tip Speed Propellers in Forward Flight, 3rd AIAA Aero-Acoustics Conference, AIAA paper 76–565, 1976/7.
[25] Morse, P. M. and Ingard, K. V.: Theoretical Acoustics, Mcgraw-Hill Book Co., Inc. New York, 1968.
[26] Guitin, L.: On the Sound Field of a Rotating Propeller, NACA TM 1195, October 1948. (Translation of "Über das Schallfeld einer rotierenden Luftschraube", Physikalishe Zeitschrift der Sowjetunion, Band 9, Heft 1, 1936, pp. 57–71.)
[27] Garrick, I. E. and Watkins, C. E.: A Theoretical Study of the Effect of Forward Speed on the Free-Space Sound-Pressure Field Around Propellers, NACA TR 1198, 1953 (Supersedes NACA TN 3018).
[28] Deming, Arthur F.: Propeller Rotation Noise Due to Torque and Thrust, NACA TN 747, 1940.
[29] Lowson, M. V.: The Sound Field for Singularities in Motion, Proceedings of Royal Society A 286, 1965, pp. 559–572.

[30] Lowson, M. V. and Ollerhead, J. B.: A Theoretical Study of Helicopter Rotor Noise, Journal of Sound and Vibration, Vol. 9, No. 2, 1969, pp. 197–222.
[31] Lowson M. V.: Basic Mechanisms of Noise Generation by Helicopters, V/STOL Aircraft and Ground Effect Machines, Journal of Sound and Vibration, Vol. 3, No. 3, 1966, pp. 454–466.
[32] Lowson, M. V.: Theoretical Analysis of Compressor Noise, The Journal of the Acoustical Society of America, Vol. 47, No. 1 (part 2), 1970.
[33] Lowson, M. V.: Waveforms for a Supersonic Rotor. Journal of Sound and Vibration, Vol. 37, No. 4, 1971, pp. 475–489.
[34] Lowson, M. V. and Hawkings, D. L.: Theory of Open Supersonic Rotor Noise, Journal of Sound and Vibration, 1974, 36 (1), 1–20.
[35] Wright, S. E.: Sound Radiation from a Lifting Rotor Generated by Asymmetric Disc Loading, Journal of Sound and Vibration, Vol. 9, No. 2, 1969, 223–240.
[36] Wright, S. E.: Discrete Radiation from Rotating Periodic Sources, Journal of Sound and Vibration, Vol. 17, No. 4, 1971, pp. 437–498.
[37] Wright, S. E.: The Acoustic Spectrum of Axial Flow Machines, Journal of Sound and Vibration, Vol. 45, No. 2, 1976, pp. 165–223.
[38] Wright, S. E.: High Forward Speed Helicopter Noise, 3rd AIAA Aero-Acoustics Conference, AIAA paper 76–562, 1976/7.
[39] Sadler, S. G. and Loewy, R. G.: A Theory for Predicting the Rotational and Vortex Noise of Lifting Rotors in Hover and Forward Flight, NASA CR–1333, 1969.
[40] Hubbard, H. H. and Maglieri, D. J.: Noise Characteristics of Helicopter Rotors at Tip Speed up to 900 Feet Per Second, The Journal of Acoustical Society of America, Vol. 32, No. 9, pp. 1105–1107, 1960/9.
[41] Cox, C. R. and Lynn, R. R.: A Study of the Origin and Means of Reducing Helicopter Noise, Bell Helicopter Co., TCREC Technical Rept. 62–73, 1962/11.
[42] Davidson, I. M. and Hargest, T. J.: Helicopter Noise, Journal of the Royal Aeronautical Society. Vol. 65, No. 5, 1965, pp. 325–336.
[43] Hargest, T. J.: Noise of VTOL Aircraft, Journal of Sound and Vibration, Vol. 4, No. 3, 1966, pp. 378–387.
[44] Widnall, Sheila E.: A Correlation of Vortex Noise Data from Helicopter Main Rotors, AIAA Journal, Vol. 6, No. 3, 1969, pp. 279–281.
[45] Lowson, M. V., Whatmore, A. R. and Whitefield, C. E.: Source Mechanisms for Rotor Noise Radiation, NASA CR–2077, 1973.
[46] Lowson, M. V. and Ollerhead, J. B.: Studies of Helicopter Rotor Noise, USAAVLABS Technical Report 68–60, 1968.
[47] Leverton, J. W.: The Noise Characteristics of a Large "Clean" Rotor, Journal of Sound and Vibration, Vol. 27, No. 3, 1973. pp. 357–376.
[48] Leverton, J. W.: Discrete Frequency Rotor Noise, AIAA 2nd Aero-Acoustics Conference, AIAA paper 75–451.
[49] Lee, A., Harris, W. L. and Widnall, S. E.: An Experimental Study of Helicopter Rotor Rotational Noise in a Wind Tunnel, 3rd AIAA Aero-Acoustics Conference, AIAA paper 76–564, 1976.
[50] Ffowcs Williams, J. E. and Hawkings, D. L.: Theory Relating to the Noise of Rotating Machinery, Journal of Sound and Vibration, Vol. 10, No. 1, 1969, pp. 10–21.
[51] Ffowcs Williams, J. E. and Hawkings, D. L.: Sound Generation by Turbulence and Surfaces in Arbitrary Motion, Philosophical Transactions of the Royal Society of London, A264, 1969, pp. 321–342.
[52] Ffowcs Williams, J. E.: Hydrodynamic noise, Annual Review of Fluid Mechanics Vol. 1, 1969.
[53] Ffowcs Williams, J. E.: The Noise from Turbulence Convected at High Speed, Phill, Trans A255 April, 1963.
[54] Jones, D. S.: The Theory of Electromagnetism, London Pergamon Press, 1964.
[55] Bryson, A. E. Jr.: An Experimental Investigation of Transonic Flow Past Two Dimensional Wedge and Circular-Arc Sections, NACA TN 2560, 1951/11.

[56] Azuma, A. and Kawachi, K.: Local Momentum Theory and It's application to the Rotary Wing, 8th AIAA Fluid and Plasma Dynamics Conference, AIAA paper, No. 75–863, 1975/6.
[57] Kasper, P. K.: Determination of Rotor Harmonic Blade Loads from Acoustic Measurements, NASA CR–2580 Oct., 1975.
[58] Hubbard, H. H. and Lassiter, L. W.: Sound from a Two-bladed Propeller at Supersonic Tip Speed, NACA Rep. 1079, 1951.
[59] Nakamura, Y.: Helicopter Noise, Ph. D. thesis, University of Tokyo, March, 1977.
[60] Lighthill, M. J.: Introduction to Fourier Analysis and Generalized Functions, Cambridge University Press, England, 1958.
[61] Gel'fand, I. M., and Shilov, G. E.: Generalized Functions. Volume 1-Property and Operations, Academic Press, 1964.